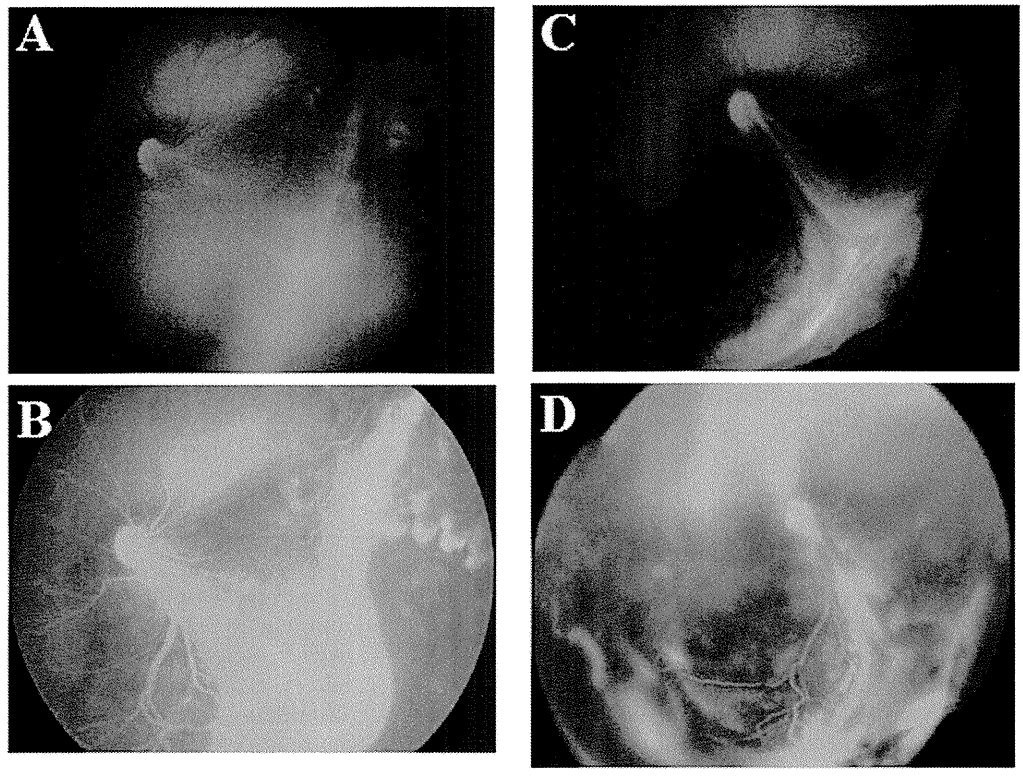

Figure 3. The left eye of patient 3 (gestational age 24 weeks; birth weight, 647 g). **A**, Preoperatively, fibrovascular tissue grows between the 2 and 8 o'clock positions and a tractional retinal detachment has developed involving the fovea (stage 4B). **B**, Severe dye leakage from the fibrovascular tissue is seen (at approximately 2 minutes and 30 seconds). **C**, Eleven days postoperatively, the retina has reattached with residual retinal folds. **D**, The dye leakage is reduced markedly with slight residual leakage (at approximately 4 minutes).

Vascular endothelial growth factor (VEGF) and other angiogenic factors contribute to the formation of neovascularization in ROP. Vitreous VEGF and stromal cell-derived factor 1α levels increase in eyes with active vascular stage 4 ROP.[16] The second essential role of early vitrectomy for APROP may be that the operation washes out angiogenic factors such as VEGF and stromal cell-derived factor 1α. Vitrectomy also seems to effectively remove the scaffold tissue and extracellular matrix that mediate angiogenesis.[17]

Recently, anti-VEGF treatment has been studied to treat ROP based on the efficacy of other angiogenic disorders such as age-related macular disease, proliferative diabetic retinopathy, and neovascular glaucoma. Intravitreal injection of bevacizumab (Avastin, Genentech, South San Francisco, CA), a recombinant humanized anti-VEGF monoclonal antibody, has been investigated for severe ROP including APROP.[18–20] The drug seems to effectively reduce vascular activity including the tunica vasculosa lentis, dilation and tortuosity of the retinal vessels, and neovascular proliferation with laser photocoagulation in early stage APROP.[18,19] Bevacizumab also may have an effect on stage 4 ROP; however, in eyes with advanced ROP, the drug cannot sufficiently reduce the vascular activity of the fibrous tissue and prevent the rapid progression of the tractional retinal detachment without vitrectomy.[20] Most important, the optimal dose of bevacizumab that preserves the normal neuroretinal development has not been determined in human ROP.[19–22] Severe ischemic retinopathies, including APROP and florid diabetic retinopathy, are followed by marked overproduction of VEGF and other angiogenic factors that lead to abnormal vascularization. Thus, 1 injection of a safe dose of bevacizumab probably cannot prevent rapid progression of the disease. Meanwhile, an intravitreal injection of bevacizumab is problematic for APROP, which is characterized by prominent fibrovascular proliferative tissue, because the drug may cause strong contraction of the fibrous tissue in advanced ROP.[23]

Early vitrectomy has a substantial effect on APROP, presumably by washing out VEGF and other angiogenic factors resulting in prompt declines in vascular activity. The positive effect on the disease may result from the complete removal of the vitreous tractional force and washing out of the VEGF and other angiogenic factors simultaneously. It is uncertain if vitrectomy can convert the active vascular stage to the inactive cicatricial stage via a change in cytokine release or if the APROP may progress spontaneously to cicatrization because of the reduced scaffolding area for the fibrovascular tissue. Further investigation is needed to clarify the mechanism of the rapid conversion of APROP to cicatrization after vitrectomy.

The current study had some limitations in that it was not randomized, controlled, or prospective to clarify whether vitrectomy with lensectomy is more appropriate to treat eyes with stage 4A APROP. Lens preservation is important to promote visual development; however, lensectomy may be necessary when the fibrovascular tissue rapidly grows to

the vitreous base in APROP. Further investigation also is needed to obtain long-term functional outcomes of early vitrectomy for APROP with continuous management of aphakic eyes.

References

1. International Committee for the Classification of Retinopathy of Prematurity. The International Classification of Retinopathy of Prematurity revisited. Arch Ophthalmol 2005;123:991–9.
2. Uemura Y, Tsukahara I, Nagata M, et al. Diagnostic and therapeutic criteria for retinopathy of prematurity [in Japanese]. Committee's Report Appointed by the Japanese Ministry of Health and Welfare. Tokyo, Japan: Japanese Ministry of Health and Welfare, 1974. Nippon no Ganka 1975;46:553–9.
3. Morizane H. Initial sign and clinical course of the most severe form of acute proliferative retrolental fibroplasia (type II) [in Japanese]. Nippon Ganka Gakkai Zasshi 1976;80:54–61.
4. Vinekar A, Trese MT, Capone A Jr, Photographic Screening for Retinopathy of Prematurity (PHOTO-ROP) Cooperative Group. Evolution of retinal detachment in posterior retinopathy of prematurity: impact on treatment approach. Am J Ophthalmol 2008;145:548–55.
5. Azuma N, Ishikawa K, Hama Y, et al. Early vitreous surgery for aggressive posterior retinopathy of prematurity. Am J Ophthalmol 2006;142:636–43.
6. Micelli Ferrari T, Furino C, Lorusso VV, et al. Three-port lens-sparing vitrectomy for aggressive posterior retinopathy of prematurity: early surgery before tractional retinal detachment appearance. Eur J Ophthalmol 2007;17:785–9.
7. Flynn JT, Cassady J, Essner D, et al. Fluorescein angiography in retrolental fibroplasia: experience from 1969–1977. Ophthalmology 1979;86:1700–23.
8. Ng EY, Lanigan B, O'Keefe M. Fundus fluorescein angiography in the screening for and management of retinopathy of prematurity. J Pediatr Ophthalmol Strabismus 2006;43:85–90.
9. Azad R, Chandra P, Khan MA, Darswal A. Role of intravenous fluorescein angiography in early detection and regression of retinopathy of prematurity. J Pediatr Ophthalmol Strabismus 2008;45:36–9.
10. Hinz BJ, de Juan E Jr, Repka MX. Scleral buckling surgery for active stage 4A retinopathy of prematurity. Ophthalmology 1998;105:1827–30.
11. Trese MT. Scleral buckling for retinopathy of prematurity. Ophthalmology 1994;101:23–6.
12. Yamashita H, Hori S, Yamamoto T. Effect of traction on the vasculature of chorioallantoic membranes of chick embryos. Invest Ophthalmol Vis Sci 1989;30:778–82.
13. Wilkinson-Berka JL, Jones D, Taylor G, et al. SB-267268, a nonpeptidic antagonist of alpha(v)beta3 and alpha(v)beta5 integrins, reduced angiogenesis and VEGF expression in a mouse model of retinopathy of prematurity. Invest Ophthalmol Vis Sci 2006;47:1600–5.
14. Albinsson S, Hellstrand P. Integration of signal pathways for stretch-dependent growth and differentiation in vascular smooth muscle. Am J Physiol Cell Physiol 2007;293:C772–82.
15. Favard C, Guyot-Argenton C, Assouline M, et al. Full panretinal photocoagulation and early vitrectomy improve prognosis of florid diabetic retinopathy. Ophthalmology 1996;103:561–74.
16. Sonmez K, Drenser KA, Capone A Jr, Trese MT. Vitreous levels of stromal cell-derived factor 1 and vascular endothelial growth factor in patients with retinopathy of prematurity. Ophthalmology 2008;115:1065–70.
17. Krishnan L, Hoying JB, Nguyen H, et al. Interaction of angiogenic microvessels with the extracellular matrix. Am J Physiol Heart Circ Physiol 2007;293:H3650–8.
18. Chung EJ, Kim JH, Ahn HS, Koh HJ. Combination of laser photocoagulation and intravitreal bevacizumab (Avastin) for aggressive zone I retinopathy of prematurity. Graefes Arch Clin Exp Ophthalmol 2007;245:1727–30.
19. Travassos A, Teixeira S, Ferreira P, et al. Intravitreal bevacizumab in aggressive posterior retinopathy of prematurity. Ophthalmic Surg Lasers Imaging 2007;38:233–7.
20. Kusaka S, Shima C, Wada K, et al. Efficacy of intravitreal injection of bevacizumab for severe retinopathy of prematurity: a pilot study. Br J Ophthalmol 2008;92:1450–5.
21. Kong L, Mintz-Hittner HA, Penland RL, et al. Intravitreal bevacizumab as anti-vascular endothelial growth factor therapy for retinopathy of prematurity: a morphologic study [letter]. Arch Ophthalmol 2008;126:1161–3.
22. Geisen P, Peterson LJ, Martiniuk D, et al. Neutralizing antibody to VEGF reduces intravitreous neovascularization and may not interfere with ongoing intraretinal vascularization in a rat model of retinopathy of prematurity. Mol Vis [serial online] 2008;14:345–57. Available at: http://www.molvis.org/molvis/v14/a43/. Accessed April 22, 2009.
23. Honda S, Hirabayashi H, Tsukahara Y, Negi A. Acute contraction of the proliferative membrane after an intravitreal injection of bevacizumab for advanced retinopathy of prematurity. Graefes Arch Clin Exp Ophthalmol 2008;246:1061–3.

Footnotes and Financial Disclosures

Originally received: December 15, 2008.
Final revision: May 7, 2009.
Accepted: May 7, 2009.
Available online: October 8, 2009. Manuscript no. 2008-1501.

The Department of Ophthalmology, National Center for Child Health and Development, Tokyo, Japan.

Financial Disclosure(s):
The authors have no proprietary or commercial interest in any of the materials discussed in this article.

Supported by Grants of Research for Disorders of Sensory Organs from the Ministry of Health Welfare and Labor, Japan.

Correspondence:
Noriyuki Azuma, MD, PhD, Department of Ophthalmology, National Center for Child Health and Development, 2-10-1 Ohkura, Setagaya-ku, Tokyo, 157-8535, Japan. E-mail: azuma-n@ncchd.go.jp.

Jpn J Ophthalmol 2009;53:12–17
DOI 10.1007/s10384-008-0602-2

CLINICAL INVESTIGATION

Age-Related Changes of Phoria Myopia in Patients with Intermittent Exotropia

Hiroshi Shimojyo[1], Yoshiyuki Kitaguchi[2], Sanae Asonuma[1], Kenji Matsushita[1], and Takashi Fujikado[2]

[1]Department of Ophthalmology, Osaka University Medical School, Osaka, Japan;
[2]Department of Applied Visual Science, Osaka University Medical School, Osaka, Japan

Abstract

Purpose: To investigate the age-related changes in a myopic shift under binocular conditions (phoria myopia) in patients with intermittent exotropia (IXT).

Methods: Forty-five patients with IXT were studied: 21 were ≤9 years old (children), 11 were between 10 and 19 years (adolescents), and 13 were between 20 and 43 years (adults). The angle of strabismus was determined by the alternating prism cover test. The spherical refractive error was measured at 1 m using infrared video retinoscopy under monocular and binocular viewing conditions.

Results: The change in the spherical refractive error (ΔR) between binocular and monocular conditions was significantly larger in adults (ΔR = –1.11 ± 1.01 diopters (D), average ± standard deviation) than in children (ΔR = –0.34 ± 0.34 D; $P < 0.05$, analysis of variance). ΔR was significantly correlated with the angle of exotropia only in adults ($r = 0.55$, $P = 0.04$). After strabismus surgery, ΔR decreased in adults ($n = 3$).

Conclusions: Because a significant myopic shift under binocular conditions was detected in IXT patients older than 20 years, phoria myopia can occur after age 20 even if functional disturbances are not observed in children or adolescent IXT patients, a fact that specialists need to bear in mind when treating younger patients. **Jpn J Ophthalmol** 2009;53:12–17 © Japanese Ophthalmological Society 2009

Key Words: aging, intermittent exotropia, myopic shift, phoria myopia, pupil constriction

Introduction

In adults with intermittent exotropia (IXT), a myopic shift and miosis are observed when the visual system switches from monocular to binocular viewing conditions.[1–5] A significant myopic shift under binocular conditions in IXT with a relatively large angle is called "phoria myopia" in Japan. Phoria myopia was first named by K. Yuge in Japanese and by K. Adachi in English.[4,5]

The miosis in the near reflex is reported to be larger in normal subjects >20 years old than in those ≤20 years.[6] However, the relationship between age and the myopic shift or pupillary constriction in patients with IXT has not been well investigated.

The relationship between convergence (C) and accommodation (A) is principally linear (AC/A or CA/C ratio) under open-loop conditions, in which either a convergence or an accommodation cue is present. However, it is not linear under closed-loop conditions, in which both cues are present. In patients with IXT, a greater effort to converge is required to fixate a near target binocularly compared with patients with orthophoria. Therefore, a greater myopic shift and miosis can be expected under exophoric (binocular) than under exotropic (monocular) conditions, especially if the angle of strabismus is large and the connection between convergence and accommodation in the central nervous system is rigid.

Received: March 5, 2008 / Accepted: July 31, 2008
Correspondence and reprint requests to: Takashi Fujikado, Department of Applied Visual Science, Osaka University Graduate School of Medicine, 2-2 Yamadaoka, Suita, Osaka 565-0871, Japan
e-mail: fujikado@ophthal.med.osaka-u.ac.jp

Recently, infrared videoretinoscopy has been developed to measure the refractive state and the pupillary size of both eyes simultaneously. This technique can be used to compare the refraction and pupillary size in exotropic and exophoric eyes. The purpose of our study was to measure the amount of myopic shift and miosis in IXT patients of different ages using an infrared videoretinoscope.

Methods

Forty-five consecutive patients with IXT who visited Osaka University Hospital in 2004 and were younger than 43 years of age were studied. Patients were included if they were able to fully participate in the examination and were able to fuse and clearly see the target binocularly. The exclusion criteria were pupil size <3 mm or refractive error beyond the limits of the instrument (i.e., >–15.0 D or >+5.0 D) in either eye. Patients with amblyopia or ocular diseases were also excluded.

All subjects gave informed consent after the purpose of this study was explained, and the procedures conformed to the tenets of the Declaration of Helsinki.

Subjects

The age of the patients ranged from 4 to 43 years. Twenty-one patients were ≤9 years old (6.5 ± 1.6 years, mean ± SD, children), 11 were between 10 and 19 years (13.5 ± 2.7 years, adolescents), and 12 were between 20 and 43 years (30.8 ± 6.0 years, adults). The best-corrected visual acuity was ≥1.0 in both eyes in all patients. None of the patients in either the children or the adolescent group complained of blurred vision or asthenopia in daily life. Four of the 12 patients in the adult group complained of blurred vision with asthenopia in daily life.

Measurements

The angle of strabismus was measured by an alternate prism cover test at 5 m. The refraction and pupillary diameter were measured simultaneously by infrared video retinoscopy and pupillography (Power Ref IIR, Plusoptix, Nürnberg, Germany). Measurements were made under both monocular and binocular viewing conditions, without spectacle correction and under mesopic light conditions. In the binocular viewing condition, the examiner monitored both eyes of each patient continuously on the Power Ref IIR screen to be certain that they fixated the target binocularly. For the monocular condition, each patient covered the left eye with his hand. The fixation target consisted of illuminated concentric circles with a diameter of 5 cm. The target distance was set at 1 m, and the results of three measurements were averaged. The average of three measurements in the right eye was used for each patient for the statistical evaluation.

Statistical Analyses

Data were statistically analyzed with SPSS 10.0J software (SPSS, Chicago, IL, USA). The data are expressed as the mean ± SD. Comparisons between two groups were made by Student's *t* test when the data were normally distributed or by the Mann-Whitney rank-sum test when the data were not normally distributed. Comparisons among groups were made by one-way analysis of variance (ANOVA) followed by the Tukey test when data were normally distributed, or one-way ANOVA on ranks when the data were not normally distributed. The age dependency of refractive or pupillary changes was analyzed by Spearman rank order correlation, and the angle dependency of the refractive or pupillary changes was analyzed by Pearson product moment correlation. Statistical significance was set at $P < 0.05$.

Results

The angle of intermittent exotropia ranged from 8 to 64 prism diopters (pd). The average angle of deviation was not significantly different among the three groups: 28.6 ± 11.1 pd in children, 21.6 ± 8.2 pd in adolescents, and 30.8 ± 6.0 pd in adults ($P = 0.23$). The spherical refractive error ranged from –6.0 to +2.5 diopters (D). The average spherical refractive error was 0.24 ± 1.38 D in children, –0.44 ± 1.69 D in adolescents, and –1.69 ± 2.61 D in adults. The spherical refractive error was significantly more myopic in adults ($P < 0.05$).

Spherical Refraction Under Monocular and Binocular Viewing Conditions

The spherical refraction under monocular, versus binocular, viewing conditions was significantly different among the three groups: 0.24 ± 1.38 D versus –0.13 ± 1.31 D ($P < 0.001$) in children; –0.44 ± 1.70 D versus –0.90 ± 1.50 D ($P < 0.003$) in adolescents; and –1.70 ± 2.61 D versus –2.80 ± 2.73 D ($P < 0.002$) in adults (Fig. 1A). We defined the myopic shift as ΔR, in which the spherical value in the binocular condition was subtracted from that in the monocular condition. The ΔR was significantly larger in adults (1.11 ± 1.01 D) than in children (0.34 ± 0.34 D; $P = 0.04$; Fig. 1B). ΔR increased with age significantly ($r = 0.334$, $P < 0.025$; Fig. 1C).

Change of Pupillary Diameter Under Monocular and Binocular Viewing Conditions

Only in adults were the pupillary diameters significantly different under binocular and monocular viewing conditions: 6.24 ± 0.80 mm versus 6.16 ± 0.66 mm ($P = 0.57$) in children; 6.18 ± 0.67 mm versus 5.89 ± 0.94 mm ($P = 0.15$) in adolescents; and 5.96 ± 0.94 mm versus 5.07 ± 1.35 mm ($P = 0.02$) in adults (Fig. 1D). The difference in the pupillary

Jpn J Ophthalmol
Vol 53: 12–17, 2009

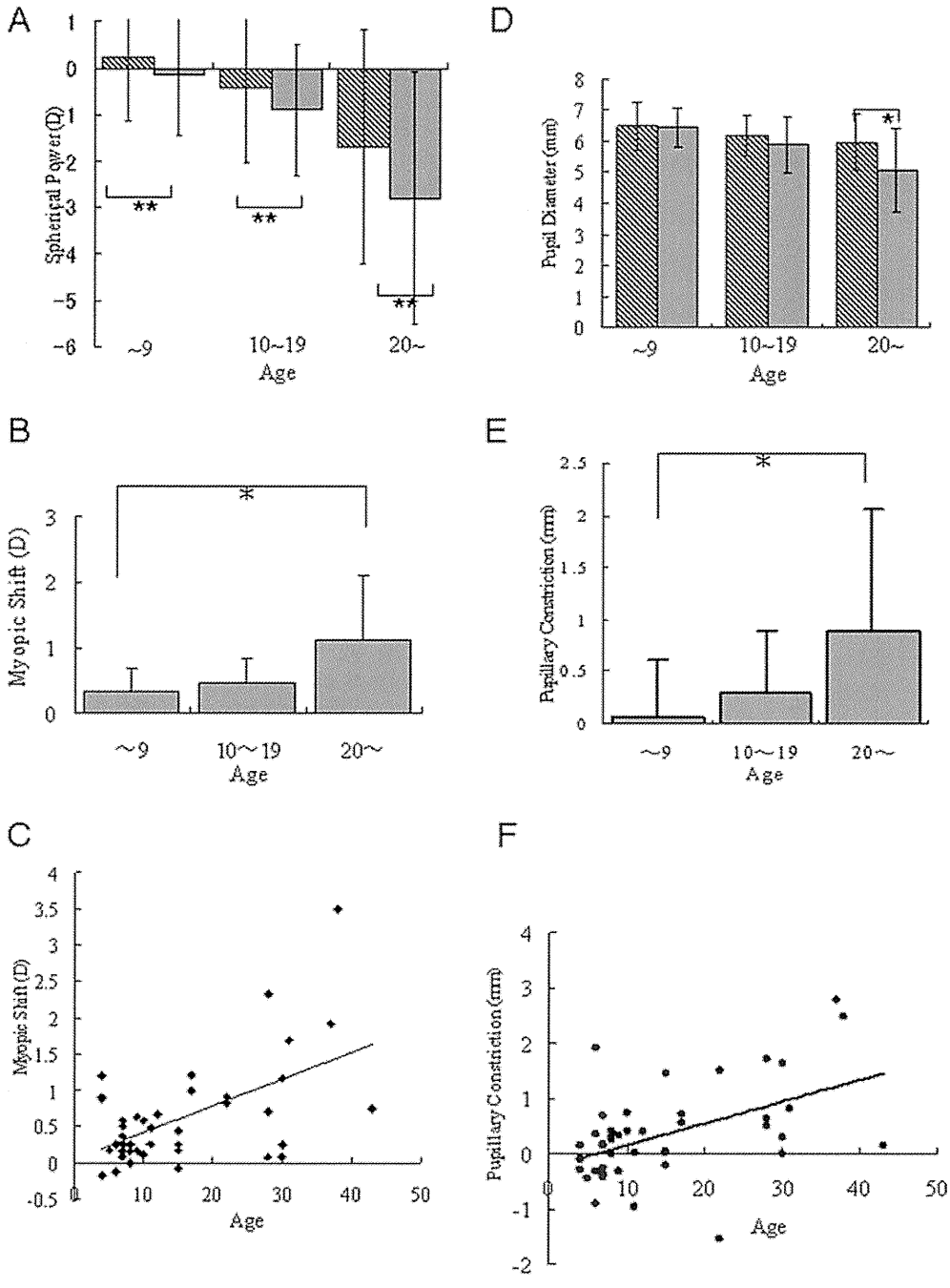

Figure 1A–F. Age-related changes of spherical refraction and pupillary diameter under monocular and binocular viewing conditions in patients with intermittent exotropia. **A** Spherical power in monocular (▨) and binocular (□) condition in different age groups. **B** Myopic shift in binocular condition in different age groups. **C** Regression of myopic shift against age. **D** Pupillary diameter under monocular (▨) and binocular (□) conditions in different age groups. **E** Pupillary constriction in binocular conditions in different age groups. **F** Regression of pupillary constriction against age. $^{**}P < 0.01$; $^{*}P < 0.05$. Bars represent the standard deviation.

diameter between monocular and binocular conditions (ΔP) was significantly greater in adults (0.89 ± 1.15 mm) than in children (0.06 ± 0.56 mm, $P = 0.02$; Fig. 1E). ΔP increased significantly with age ($r = 0.495$, $P < 0.001$; Fig. 1F).

Relationship Between ΔR and the Angle of Strabismus

In adults, the correlation between ΔR and the angle of strabismus was significant ($r = 0.55$, $P = 0.04$), but it was not significant in children ($r = -0.20$, $P = 0.40$) or adolescents ($r = 0.10$, $P = 0.66$) (Fig. 2A–C).

Relationship Between ΔP and the Angle of Strabismus

The correlation between ΔP and the angle of strabismus was not significant in adults ($r = 0.46$, $P = 0.11$), children ($r = 0.10$, $P = 0.66$), or adolescents ($r = 0.05$, $P = 0.89$) (Fig. 2D–F).

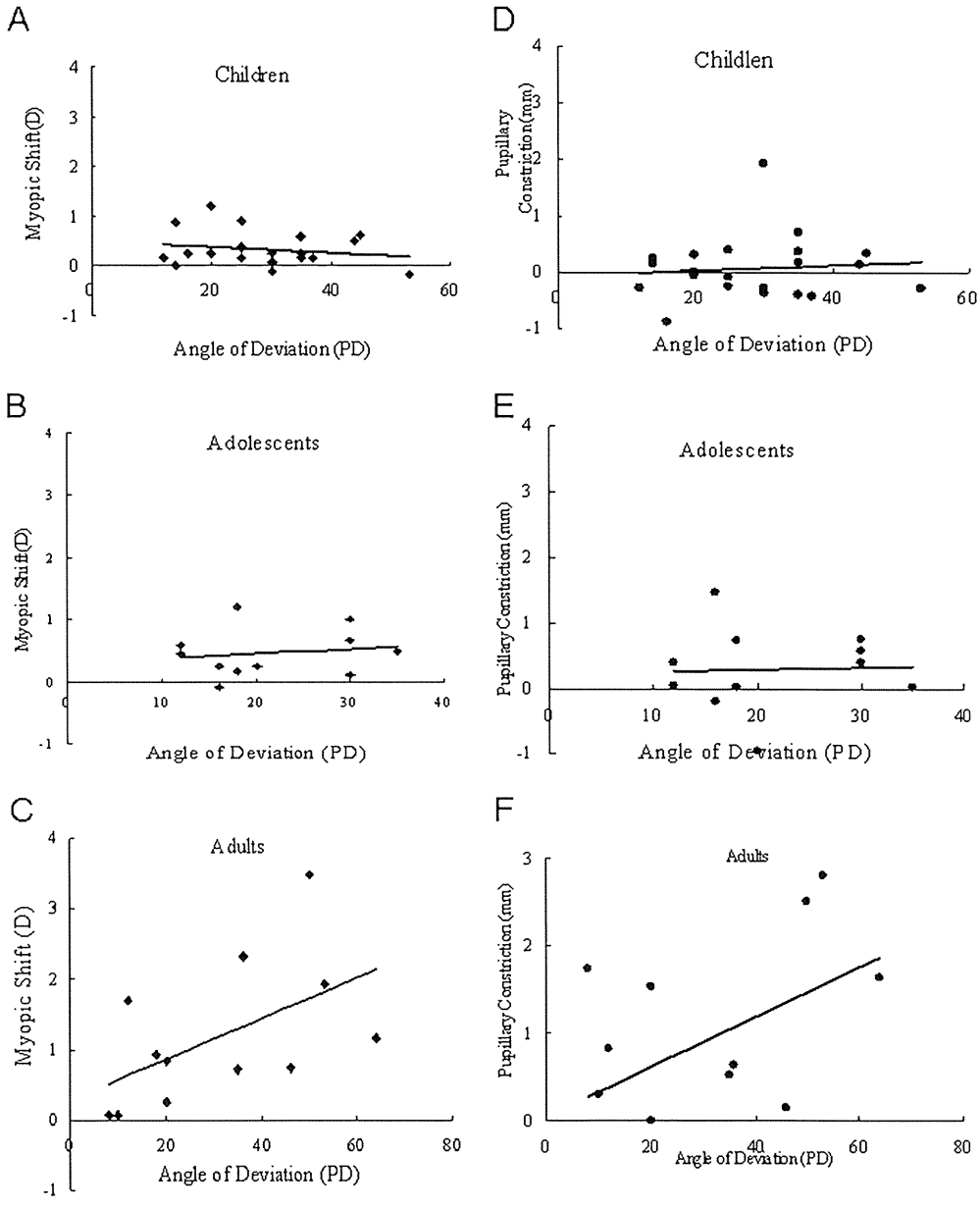

Figure 2A–F. Correlations of myopic shift (**A–C**) and pupillary constriction (**D–F**) with angle of strabismus. **A, D** Children (4–9 years of age). **B, E** Adolescents (10–19 years of age). **C, F** Adults (20–43 years of age).

Change of Spherical Refraction and Pupil Diameter After Strabismus Surgery in Adults

Three patients in the adult group underwent strabismus surgery (patients 1–3). Their ages were 28, 30, and 38 years. The angle of exotropia at 5 m was 36, 54, and 50 pd, respectively, before strabismus surgery, which improved to 20, 30, and 35 pd, respectively, after surgery (Fig. 3A). ΔR was 2.3, 1.2, and 4.6 D, respectively, before strabismus surgery and decreased to 0.4, 0.6, and 3.5 D, respectively, after surgery. ΔP was 0.6, 1.6, and 3.1 mm, respectively, before strabismus surgery and decreased to 0.3, 0.9, and 2.2 mm, respectively, after surgery. Patients 1 and 2 had blurred vision when they fixated binocularly before surgery, and the blurring disappeared after surgery.

Discussion

Our results showed that a significant myopic shift occurred not only in adults but also in children and adolescents (Fig. 1A). However, the myopic shift was less than 0.5 D in children and adolescents (Fig. 1B), so the mean myopic shift was most likely within the depth of focus of the eye. The amplitude of the myopic shift was significantly larger in adults than in children (Fig. 1B, C). These findings indicate that a large myopic shift (phoria myopia) occurred only in adults.[5]

The change in the pupillary diameter under binocular viewing conditions was not significantly different from that under monocular conditions in children or adolescents (Fig. 1D), and the change in the pupillary diameter was

Jpn J Ophthalmol
Vol 53: 12–17, 2009

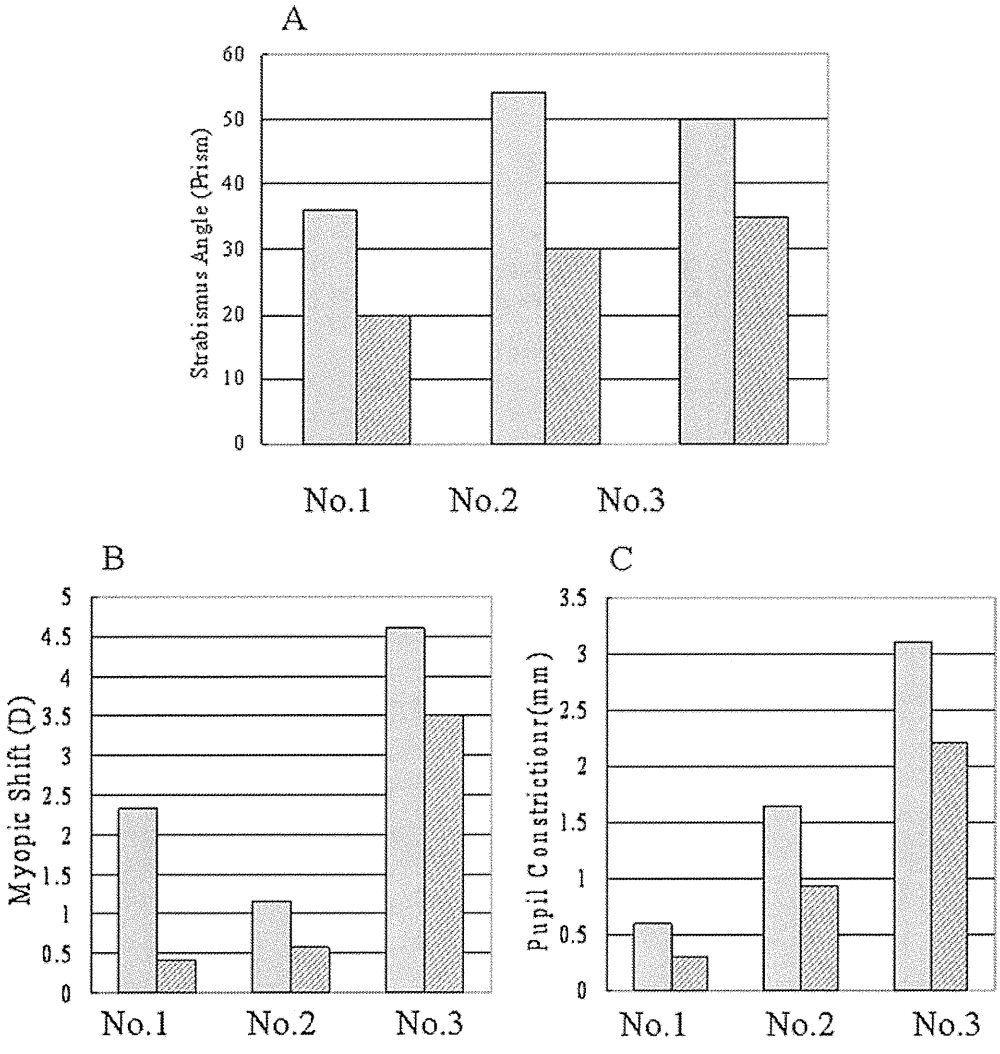

Figure 3A–C. Angle of strabismus (**A**), myopic shift (**B**), and pupil constriction (**C**) before (□) and after (▨) strabismus surgery in three adult patients with intermittent exotropia.

significantly larger in adults than in children or adolescents (Fig. 1E, F). These findings are consistent with a report that the pupillary near response is very small in subjects younger than 20 years and significantly larger in adults.[6]

The relationship between the change of spherical refraction and the angle of strabismus was distinctly different in adults compared with that in children and adolescents (Fig. 2A–C). In the adults, a significant correlation was observed between ΔR and the angle of strabismus, whereas the correlation was very weak in children and adolescents. These results again indicate that phoria myopia occurs only in adult IXT patients. The correlation between pupil constriction and the angle of strabismus was not statistically significant in any of the groups but showed a similar tendency as that between the myopic shift and the angle of strabismus in adults.

The degree to which fusional convergence influences accommodation is defined as the convergence accommodation to convergence (CA/C) ratio under open-loop accommodation conditions. A recent study has shown that the CA/C ratio decreases with age,[7] but the degree of myopic shift increases with age, especially in adults under closed-loop conditions. This suggests the presence of a factor that reduces the convergence accommodation under closed-loop conditions, while patients are still young. This can, for example, be explained by the presence of a control system model of cross-linked interactions between accommodation and convergence.[8–10]

In this model, accommodation has both a phasic and a tonic response. The former is a fast response that causes convergence accommodation, and the latter is a slow adaptable response that gradually replaces the phasic response.[8] The results of our study suggest that in patients over 20 years of age, the tonic response may be reduced, leading to an increase in the amplitude of convergence accommodation under closed-loop conditions.

The baseline refraction obtained under monocular conditions was more myopic in adults than in children. The response may not have differed among the three groups because the target was set at 1 m, although the baseline refraction was more myopic in adults.

Reducing the exodeviation by surgery not only improves binocular vision but also reduces the associated myopic shift and pupillary constrictions (Fig. 3). Although patients complained of blurred vision when they fixated binocularly before surgery, this complaint disappeared after surgery.

In conclusion, a considerable myopic shift with miosis occurred under binocular conditions in adult IXT patients. The blurred vision under binocular viewing conditions induced by the myopic shift improved after strabismus surgery. These results suggest that even if functional disturbances are not observed in children or adolescent IXT patients, phoria myopia can still occur in patients older than 20 years.

Acknowledgments. This study was supported by a Health Sciences Research Grant (H18-sensory-06) from the Ministry of Health, Labour and Welfare, Japan.

References

1. Bielshowski A. Exo Phorieud "Divergenzexzess". Klin Augenheilkd 1934;92:11–28.
2. Burian, Hermann M. Intermittent (facultative) divergent strabismus: its influence on visual acuity and the binocular visual act. Am J Ophthalmol 1945;28:525–527.
3. Seaber JH. Pseudomyopia in exodeviations. Am Orthoptic J 1966;16:67–72.
4. Yuge K. Starabismus and amblyopia (in Japanese). Tokyo: Nanzando; 1963. p 79.
5. Adachi K. Refraction in relation to strabismus (in Japanese). Kyoto Gankaikai Kaiho 1980;3:3.
6. Wilhelm H, Schaeffel F, Wilhelm B. Die Altersabhangigkeit der Pupillennahreaktion. Klin Monatsbl Augenheilkd 1993;203:110–116.
7. Nonaka F, Hasebe S, Ohtsuki H. Convergence accommodation to convergence (CA/C) ratio in patients with intermittent exotropia and decompensated exophoria. Jpn J Ophthalmol 2004;48:300–305.
8. Schor CM. The influence of interactions between accommodation and convergence on the lag of accommodation. Ophthalmic Physiol Opt 1999;19:134–150.
9. Hasebe S, Nonaka F, Otsuki H. Accuracy of accommodation in heterophoric patients: testing an interaction model in a large sample. Ophthalmic Physiol Opt 2005;25:582–591.
10. Rosenfield M, Ciuffreda KJ, Chen HW. Effect of age on the interaction between the AC/A and CA/C ratios. Opthalmic Physiol Opt 1995;15:451–455.

Clinical Application of Autofluorescence Densitometry with a Scanning Laser Ophthalmoscope

Tetsuju Sekiryu,[1] *Tomohiro Iida,*[1] *Ichiro Maruko,*[1] *and Masayuki Horiguchi*[2]

Purpose. Fundus autofluorescence (FAF) affects the overlying absorptive retinal pigments within the eye and can potentially be used to assess their density. This study reports a clinical application of FAF in measuring photopigments by scanning laser ophthalmoscopy (SLO).

Methods. The study group comprised 20 healthy subjects, 4 patients with branch retinal artery occlusion (BRAO), 3 with macular hole, 3 with branch retinal vein occlusion (BRVO), and 4 with resolved central serous chorioretinopathy (CSC). Serial FAF images were taken during exposure to light. The intensity of the FAF was measured at the site of the macular hole or the photocoagulation laser burn in the eyes with BRVO. The autofluorescence optical density difference (fODD) was measured from the FAF images and mapped to elucidate the topographic pattern.

Results. The autofluorescence intensity showed little change at the sites of the macular holes or photocoagulation burns during exposure to light. The fODD was smallest at the center of the fovea and gradually increased with the eccentricity within 270 × 270 pixels around the fovea in healthy subjects. The amplitude of the fODD did not change in the area affected with BRAO in comparison to the unaffected area. By contrast, the fODD decreased in the area of resolved serous retinal detachment in the eyes with CSC.

Conclusions. In eyes with retinal disease, measuring the autofluorescence intensity using SLO is a feasible method of assessing the changes in the photopigments. Further studies comparing this approach with conventional methods for examining photopigments are needed. (*Invest Ophthalmol Vis Sci.* 2009;50:2994–3002) DOI:10.1167/iovs.08-2774

Fundus autofluorescence (FAF) imaging is playing increasingly important roles in diagnosing age-related macular degeneration and macular dystrophies.[1–4] FAF is generated by retinal pigment epithelium (RPE) lipofuscin,[5] which is a mixture of fluorophores that represent the digested residues of the retinal outer segments.[6] Previous studies have reported that FAF is influenced by the overlying retina.[5,7,8] The intensity of FAF may be altered by the bleaching of photopigments. Reflection densitometry is the only objective method for investigating visual photopigments in a living eye.[9–16] The possibility of applying FAF to densitometry has been suggested in a previous report.[17] The recently developed scanning laser ophthalmoscope HRA2 (Heidelberg Engineering, Heidelberg, Germany) makes it possible to observe changes in the FAF during exposure to light (Fig. 1). FAF with the HRA2 can be applied to the imaging densitometry of autofluorescence. Imaging densitometry has the advantage of assessing the topographical changes of human photopigments compared with single-spot densitometry.[13,18] Unlike in reflectometry with scanning laser ophthalmoscopy (SLO), in densitometry using FAF, the optical crosstalk caused by the surface of the retina and the choroid is thought to be relatively minor. However, the distribution of lipofuscin and macular pigments, pathologic changes of the RPE, and the thickness of the sensory retina may all contribute to the FAF intensity during exposure to light. The relationships between these factors and autofluorescence intensity must be known to determine the efficacy of autofluorescence densitometry. We studied the characteristics of autofluorescence optical density differences caused by photopigments using the HRA2 system.

Methods

Population

FAF images were obtained from 20 subjects (4 women and 16 men; mean age, 56 years; age range, 26–73) who were free of retinal diseases or significant cataract and corneal opacity. These individuals did not have any general diseases with the exception of hypertension. All the subjects were Japanese. No pseudophakic or aphakic eyes were included in this group. For each subject, two sessions on the same eye were conducted, more than 1 month apart. Images were acquired from only one eye per session. The FAF of the eyes with fundus diseases was also examined to illustrate the characteristics of autofluorescence optical density differences in various retinal lesions. These diseases included stage 4 macular hole (n = 3), long-standing branch retinal artery occlusion (BRAO; n = 4), and central serous chorioretinopathy (CSC; n = 4). To assess photocoagulated burns, we examined three patients with old branch retinal vein occlusion (BRVO; n = 3). The eligible patients with BRAO and BRVO from 6 to 24 months after onset had little retinal edema and retinal hemorrhage. In the patients with CSC 6 months or more after onset, serous retinal detachment (SRD) was completely resolved. We assessed the photoreceptor inner/outer segment junction (IS/OS) with optical coherence tomography (OCT) at the time of the examination. The IS/OS was well preserved in the eyes with BRAO. In the eyes with BRVO and CSC, the OCT IS/OS was disturbed in the fovea of the affected area of SRD. The tenets of the Declaration of Helsinki were observed. The Institutional Review Board of the University of Fukushima Medical School, Japan, granted approval for this project. Informed consent was obtained from all subjects and patients.

Retinal Imaging

The FAF images were recorded with an HRA2 confocal scanning laser ophthalmoscope. The wavelength of excitation was 488 nm (0.2 mW at the cornea). The detection filter transmitted light at wavelengths >500 nm. The size of the image field was 30°×30° (768 × 768 pixels). We took care to ensure that all the images covered the optic disc and the macula. The subjects were dark-adapted for 30 minutes. After achieving the required eye alignment and focusing in the infrared mode, serial FAF images were taken at a rate of 4.7 Hz for eyes with dilated pupils during a period of >40 seconds from the beginning of the acquisition. During image acquisition, the fundus was exposed to laser illumination. All the subjects and patients were instructed to gaze intensely at the external

From the [1]Department of Ophthalmology, Fukushima Medical University School of Medicine, Fukushima, Japan; and the [2]Department of Ophthalmology, Fujita Health University, Aichi, Japan.

Submitted for publication August 27, 2008; revised December 17, 2008; accepted April 13, 2009.

Disclosure: **T. Sekiryu**, None; **T. Iida**, None; **I. Maruko**, None; **M. Horiguchi**, None

The publication costs of this article were defrayed in part by page charge payment. This article must therefore be marked "*advertisement*" in accordance with 18 U.S.C. §1734 solely to indicate this fact.

Corresponding author: Tetsuju Sekiryu, 960-1295, 1 Hikarigaoka, Fukushima City, Fukushima Pref., Japan; sekiryu@fmu.ac.jp.

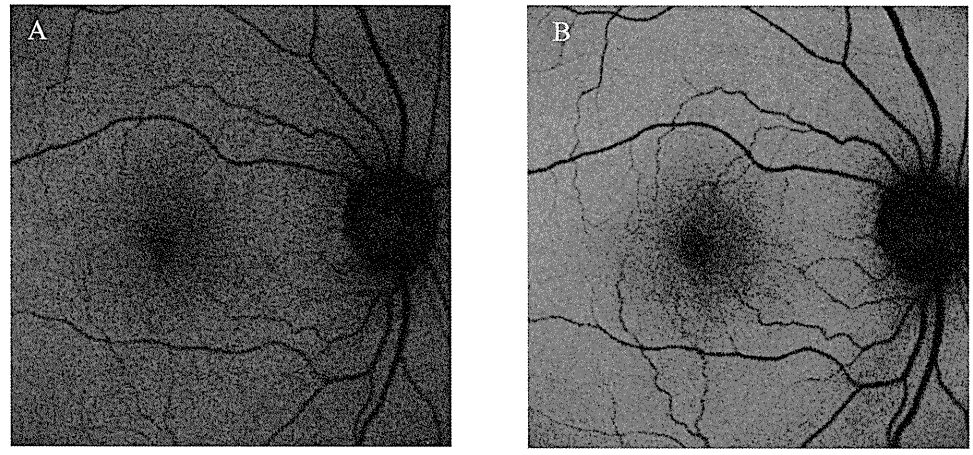

FIGURE 1. Changes of autofluorescence images caused by exposure to light. (**A**) Autofluorescence image at the beginning of observation using HRA2. (**B**) Autofluorescence image after a 40-second observation. The intensity of autofluorescence was increased by the bleaching of photopigments.

fixation light with the fellow eye (that is, the eye that was not being examined). The layer structure of the retina was examined by spectral domain (SD)-OCT using the 3D-OCT-TM system (Topcon, Tokyo, Japan) and Cirus-TM HD-OCT (Carl Zeiss Meditec, Jena, Germany).

Image Analysis

Before analysis, the serial FAF images were aligned to fix the viewpoint by using the software installed in the HRA2 system. The movie files were output as AVI files for the measurements. The FAF intensity in the macular holes and areas affected by laser coagulation therapy was measured after setting the square region of interest within these areas.

To measure the distribution of the FAF intensity, 9 × 9 grids of 30 × 30 pixels were allocated to the image of the fovea. The center of the grid was aligned at the darkest point in the fovea on the last of the serial images (Fig. 2A). The intensity of each point was measured as an eight-bit grayscale value on the frame of the AVI file (Glay-bal; Liberally Inc., Tokyo, Japan). Eye movement and blinking caused nonuniform illumination and regional variations of the autofluorescence intensity; these data were excluded from the analysis. To correct the slow intensity change during the image acquisition, the difference of the intensity of the vessels at the disc rim during the session was subtracted from the reading value of each grid.

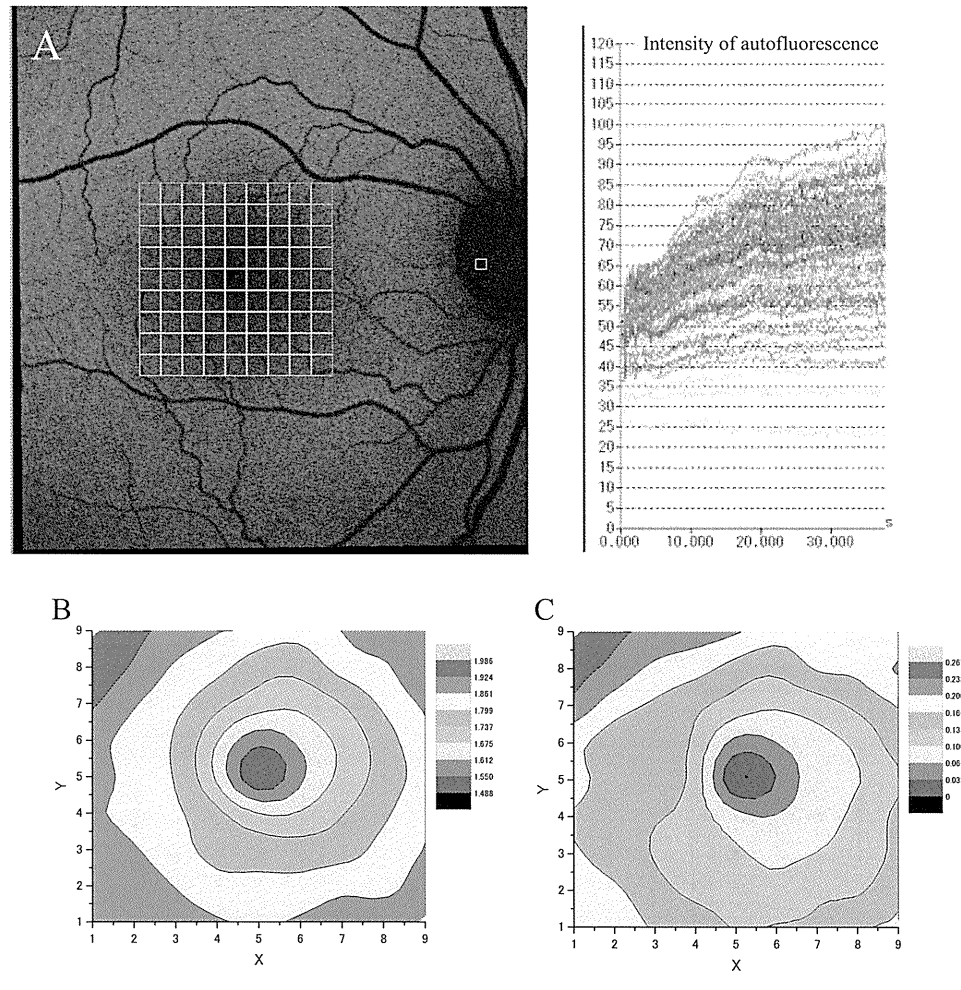

FIGURE 2. Measurement in normal subjects. (**A**) Display image of the measurement of autofluorescence intensity. The mean intensity in each cell of the 9 × 9 grid was measured and fitted to the exponential formula. (**B**, **C**) False-color maps of isointensity contours of log[*F*(end)] (**B**) and fODD (**C**). The maps were created by interpolating across each grid and assigning different colors automatically. Log[*F*(end)] was the actual value measured at the end of the measurement. fODD was calculated by fitting the logarithm of autofluorescence to equation 2.

Data Analysis

To estimate the ODD, the grayscale value during exposure to light was fitted to the following formula. During bleaching, the fraction of photopigments can change in an exponential fashion.[9,11] The intensity of FAF at time t was described as

$$F(t) = F(\infty) \times 10^{[-\mathrm{fODD} \times \exp(-kt)]} \quad (1)$$

where $F(t)$ is the measured autofluorescence at time t, $F(\infty)$ is the autofluorescence at an infinite time when the $F(t)$ approaches a constant level, fODD is the optical density difference of the pigment between the dark-adapted density and the density of the pigment after an infinitely long duration, and k is the time constant relating the chromophore properties and the intensity of light at the site of measurement. After taking the log of both sides,

$$\log[F(t)] = \log[F(\infty)] - \mathrm{fODD} \times \exp(-kt) \quad (2)$$

we fitted the logarithmic value of the FAF intensity to equation 2 on a least-squares basis with the Levenberg-Marquardt method, which gives the three unknown parameters (log[$F(\infty)$], fODD, and k), with commercial computer software (Origin 8; OriginLab Corp., Northampton, MA). In this method, log[$F(\infty)$] is calculated by extrapolation. The fODD is given as the value when the log(F) reaches a constant level. The results were displayed using a contour map classified into 11 phases. When the intensity of autofluorescence decreased or the change of the autofluorescence intensity was too small to fit equation 2 at the site of measurement, the fODD of the site was treated as 0.

To compare the distribution of FAF, the logarithmic value of the grayscale at the end of the measurement (log[F(end)]) was mapped in the same manner. The value of log[F(end)] was the actual value near log[$F(\infty)$], but was not the same as log[$F(\infty)$].

Statistical Methods

The differences of log[$F(\infty)$], fODD, and k at the temporal fourth grid in two sessions were analyzed by the paired t-test. To evaluate the symmetry of the intensity of FAF (log[F(end)] and the fODD, we compared the mean and SD at the symmetrical site of the grid on vertical and horizontal lines through the center of the fovea. The difference at the symmetrical site was tested by the paired t-test.

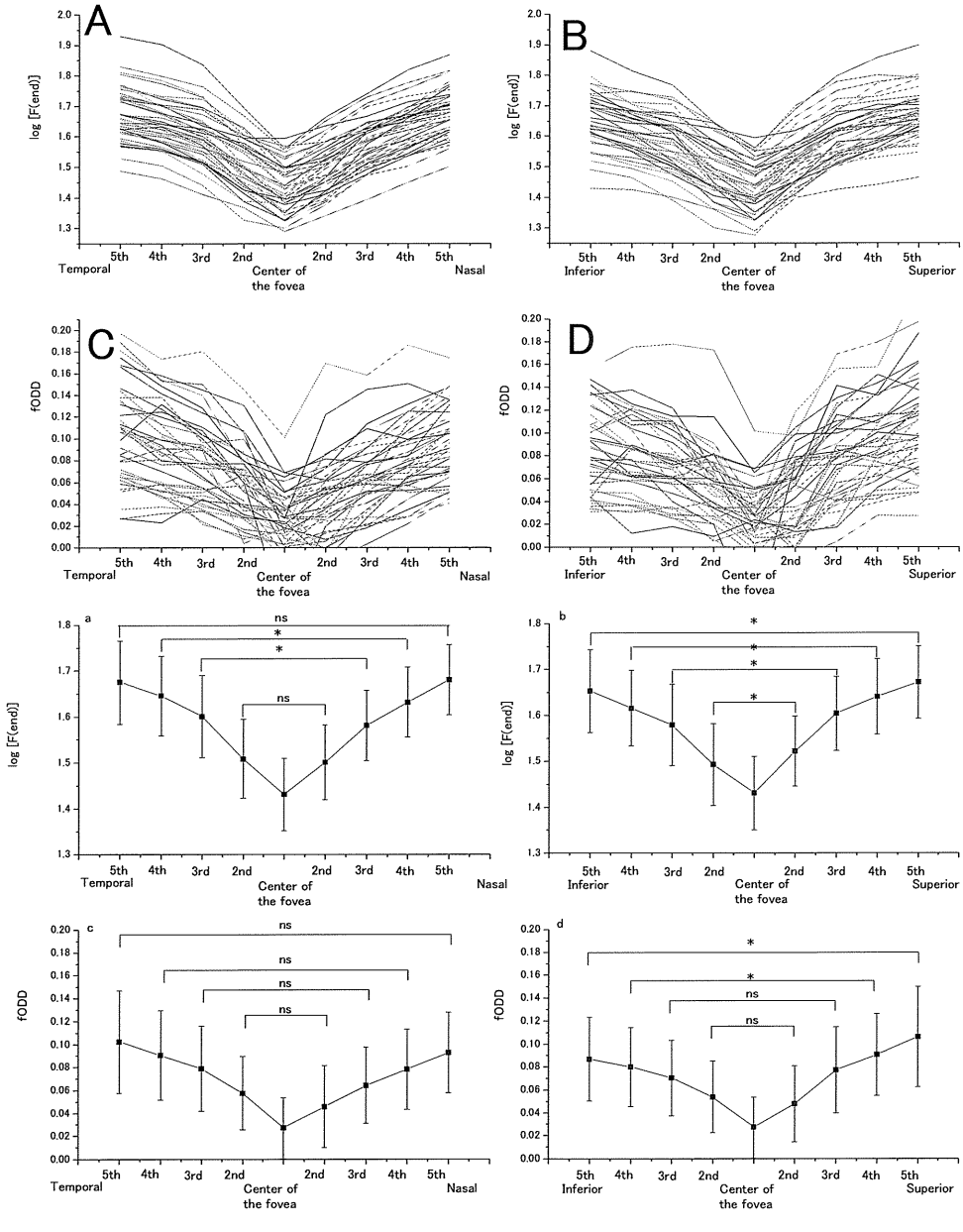

FIGURE 3. Vertical and horizontal distributions of log[F(end)] and fODD throughout the session. (**A**) Horizontal distribution of log[F(end)]. (**B**) Vertical distribution of log[F(end)]. (**C**) Horizontal distribution of fODD. (**D**) Vertical distribution of fODD. (**a–d**) The mean of (**A–D**), respectively. *Vertical lines* show the SD. At the fourth grid from the center of the fovea, the intensity of FAF was seen temporally, followed by nasally, superiorly, and inferiorly. The mean fODD was significantly higher superiorly than inferiorly. $^*P < 0.05$.

TABLE 1. Intensity of Autofluorescence in the Fourth Grid Temporal to the Fovea in a Total of 40 Sessions in 20 Normal Subjects

	1st Session			2nd Session		
Case	log($F\infty$)	fODD	k	log($F\infty$)	fODD	k
1	1.5551	0.0210	0.0580	1.5540	0.0372	0.0499
2	1.5563	0.0350	0.0585	1.5798	0.0473	0.0569
3	1.5820	0.0544	0.0617	1.5871	0.0602	0.0682
4	1.6627	0.0652	0.1613	1.6712	0.0580	0.1465
5	1.8006	0.0649	0.0669	1.7838	0.0940	0.0624
6	1.6353	0.0948	0.0763	1.6220	0.0868	0.0884
7	1.6023	0.1019	0.0791	1.6073	0.0840	0.0668
8	1.5950	0.0643	0.0621	1.5984	0.0809	0.0556
9	1.6404	0.1023	0.0608	1.6610	0.0988	0.0571
10	1.6972	0.0953	0.1656	1.6805	0.1131	0.0517
11	1.7072	0.1027	0.0684	1.7035	0.1245	0.0652
12	1.7258	0.1028	0.0668	1.7233	0.1273	0.0717
13	1.7168	0.1260	0.0675	1.7295	0.0992	0.0565
14	1.4581	0.1362	0.0561	1.5046	0.0580	0.0520
15	1.7120	0.1517	0.0696	1.6948	0.1532	0.0757
16	1.9072	0.1520	0.0675	1.8828	0.1581	0.0708
17	1.5716	0.1418	0.0755	1.6011	0.1483	0.0880
18	1.6228	0.0874	0.0522	1.6113	0.0762	0.0418
19	1.5549	0.1145	0.1051	1.5591	0.0937	0.1245
20	1.6731	0.1156	0.0612	1.6805	0.1131	0.0517
Ave	1.6488	0.0965	0.0770	1.6518	0.0956	0.0701
Std	0.100	0.037	0.032	0.088	0.035	0.026

The vertical and horizontal distribution is shown in Figure 3. Log[F(end)] is the logarithmic value of the grayscale at the end of the measurement. fODD is the optical density difference in FAF. k is the time constant. There was no significant difference between the two sessions according to the paired t-test. t = 0.464 [log($F\infty$)], 0.868 (fODD), and 0.2610 (k).

RESULTS

The autofluorescence intensity increased during exposure to laser light in the normal eyes (Fig. 1). The background of FAF at the beginning of acquisition was dark (Fig. 1A). The retinal vessels were clearly delineated at the end of acquisition, depending on the increase in the intensity of the background.

Healthy Subjects

Summaries of the vertical and horizontal distributions of the peak autofluorescence intensity (log[F(end)]) and the fODD are shown in Figure 3. The grayscale value at the site of measurement was corrected by the grayscale value of the disc in the same frame, which was considered to be almost constant during exposure to light. The intensity of autofluorescence (log[F(end)]) was lowest at the center of the fovea and increased gradually toward the periphery within a 270-pixel square. At the fourth grid from the center of the fovea, the intensity of FAF was seen temporally, followed by nasally, superiorly, and inferiorly. The difference in logarithmic intensity between the center of the fovea and the temporal fifth grid was 0.244 ± 0.063.

The fODD was generated by fitting to a simple exponential formula, equation 2. The fODD was smallest at the center of the contiguous eight grids. The mean fODDs were too small to fit the curve in 12 (30%) of the 40 sessions in the 20 normal eyes. In comparison with the symmetrical positions of the grids, the mean fODDs did not differ between the horizontal grids. The mean fODDs were significantly higher superiorly than inferiorly. The k value showed various distributions, rather than a specific distribution. In false-color maps of the isointensity contours of autofluorescence in the bleached state, the distribution of the log[F(end)] value showed a concentric pattern (Fig. 2B). The fODD increased gradually with the eccentricity within a 270-pixel square, but the pattern was not the same as the autofluorescence distribution (Fig. 2C). The fitting results of log[$F(\infty)$], k, and fODD were calculated at the point of the fourth grid temporal to the fovea in two sessions (Table 1). There was no significant difference between the two sessions according to the paired t-test; t was 0.464 (log($F\infty$)), 0.868 (fODD), and 0.2610 (k). Overall, for the 40 sessions, the mean ± SD values of log[$F(\infty)$], fODD, and k were 1.65 ± 0.093, 0.096 ± 0.035, and 0.073 ± 0.029, respectively.

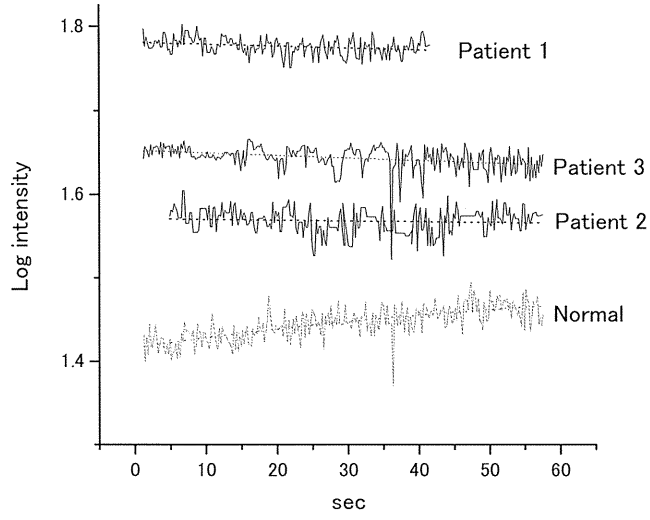

FIGURE 4. Logarithmic value of autofluorescence during exposure to light in the macular hole of three eyes from three patients. *Three black solid lines*: the logarithm of the grayscale value during exposure to light. *Dashed lines*: linear regression curves (data shown in Table 2). *Gray line*: logarithm measured at the center of the fovea in the subject shown in Figure 2, which is presented as a normal reference. The intensity of autofluorescence in the macular hole was high at the beginning of the measurement period and decreased slightly during exposure to light compared with a normal subject. The mean values of the slope of the linear regression curve for the three patients were −0.00022, −0.00009, and −0.00030, respectively.

Eyes with Diseases

Patients with macular hole showed high autofluorescence intensity compared with normal subjects at the beginning of the measurement period, which did not increase significantly during exposure to light (Fig. 4). The mean values of the slope of the linear regression curve for the three patients were −0.00022, −0.00009, and −0.00030, respectively (Table 2).

TABLE 2. Coefficient of Linear Regression Curve of Logarithm of FAF Shown in Figure 4

Patient	y Intercept	SE	Slope	SE	Fit to Eq. 2
1	1.78098	0.00144	−0.00022	5.88E-05	Failed
2	1.57071	0.0021	−0.00009	6.04E-05	Failed
3	1.65247	0.00168	−0.00030	5.01E-05	Failed
Average	1.67084	0.00339	−0.00039	1.40E-04	Failed
Normal	1.42043	0.00172	0.00085	0.00005	Success

The normal data represents the autofluorescence intensity change at the center of the fovea in the eye shown in Figure 2 and were fitted to the linear regression curve to compare the data. The fitting to the exponential formula failed in three patients with macular hole.

* Fit to Eq. 2, resultant fitting of logarithmic autofluorescence to equation 2.

The three patients with BRVO underwent laser coagulation of the affected area with a yellow laser (Multicolor Laser; Nidek, Gamagori, Japan). The fODD was decreased in the affected area with BRVO. In a 63-year-old man, the IS/OS line was distinguishable in this area, although the intensity of the intermediate line between the IS/OS line and the RPE line decreased (Figs. 5E, 5G). The FAF intensity was measured in the linearly aligned grids through the laser burn. The FAF intensity increased in the area outside of the photocoagulation burn near the vascular arcade. At the sites of the burns, the change in autofluorescence intensity during exposure to light was too slight to fit to equation 2, where SD-OCT revealed a clearly delineated IS/OS line (Figs. 5H, 5I). The change in FAF intensity after 13 of the 15 laser burns was too small to fit equation 2 (86.7%). Bleaching of the photoreceptor was not detected in most of the laser burns showing a defect of the IS/OS line.

The retina was atrophic in the affected area of eyes with long-standing BRAO at more than 3 months after onset. In a 33-year-old man, the layer structure of the inner retina disappeared on the SD-OCT images. However, the IS/OS line was well preserved. The map of the fODD demonstrated concentric patterns in the four eyes with BRAO (Fig. 6).

The fODD was measured in the four eyes with resolved CSC more than 6 months after onset. The map of the fODD was depressed in the area corresponding to the affected region of SRD, although the map of log[*F*(end)] showed hyperautofluorescence in this area. SD-OCT revealed that the IS/OS line was attenuated within the affected region (Fig. 7). The response of multifocal ERG also decreased in the inferior fovea where the fODD decreased.

The characteristics of the fODD are summarized in Table 3.

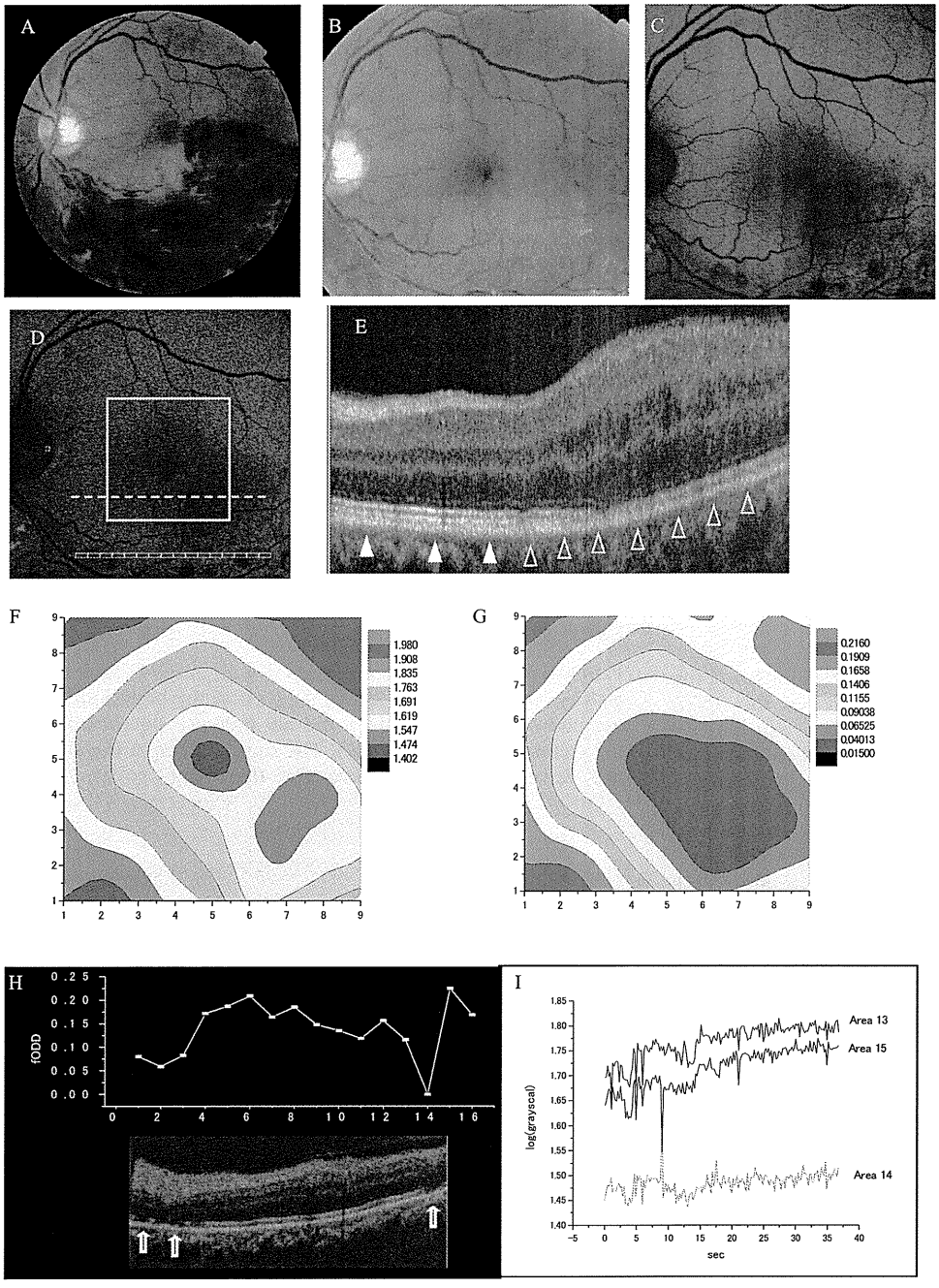

FIGURE 5. Changes of autofluorescence on laser burn in an eye with BRVO in a 63-year-old man. (**A**) Color fundus photograph at the first visit. (**B**) Color fundus photograph 10 months after onset. The hemorrhage was resolved, and laser photocoagulation burns were seen near the vascular arcade. (**C**) Image of FAF taken 10 months after onset. The intensity of autofluorescence decreased at the edge of the burns. The center of the burns showed weak autofluorescence. (**D**) The *large square* around the fovea shows the range of the measured optical density difference in (**G**). *Dashed line*: the position scanned by SD-OCT in (**E**). The 16 *small squares* near the vascular arcade indicate the positions scanned by SD-OCT and measured for fODD in (**H**) and (**I**). (**E**) SD-OCT image. The intermediate line is clearly delineated in the healthy area (*white arrowheads*). The intensity of the intermediate line decreased in the affected area (*open arrowheads*). (**F**) Color map of log[*F*(end)]. (**G**) Color map of fODD. The fODD decreased in the area affected by BRVO. (**H**) Graph showing the fODD in the 16 linearly aligned areas across the laser burn. The SD-OCT image shows the retinal tomography corresponding to the 16 areas where the fODD was measured. *White arrows*: laser burns. fODD decreased in the affected regions (areas 8–13). The laser burns (areas 2, 3, and 14) showed a further decrease of the fODD compared with the surrounding area. (**I**) The intensity of autofluorescence changed during exposure to light in areas 13 to 15. The intensity was converted to the logarithmic value. The intensity in the laser burn region (area 14) was not increased by exposure to light.

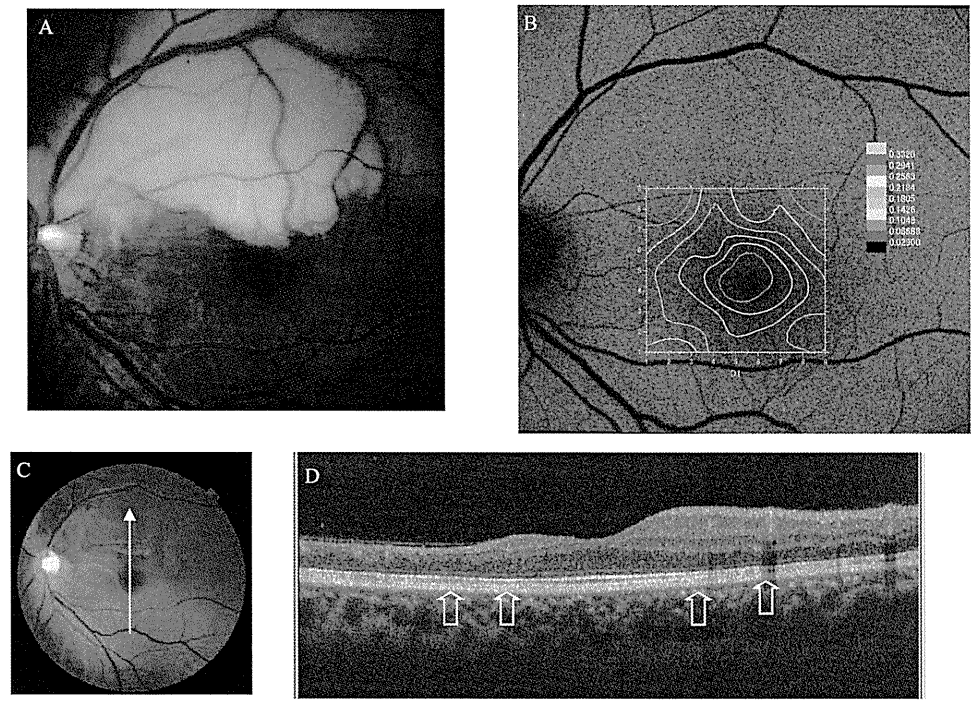

FIGURE 6. A 33-year-old patient with BRAO. (**A**) Color fundus photograph at onset. (**B**) Map of fODD overlapped with FAF image at the examination 5 months after onset. The concentric pattern of the contour map indicated that the fODD of the affected area did not decrease. (**C**) Fundus color photograph 5 months after onset. *White arrow*: the direction of the OCT scan. (**D**) The vertical OCT scan shows atrophy of the sensory retina in the affected area. The IS/OS band is not damaged even in the affected area. *Arrows*: the IS/OS line.

DISCUSSION

FAF is a useful tool for diagnosing hereditary diseases and investigating macular disorders.[3,19,20] Because autofluorescence generated by the RPE cells travels through the sensory retina, the intensity of the FAF changes according to the status of the overlying retina.[7,8] Although a change in FAF due to bleaching was reported previously,[5,17,21] this measurement has not been applied clinically. In the present study, we used autofluorescence from the RPE to evaluate photopigments, using the HRA2 (Heidelberg Engineering).

Technique

The HRA2 provides high-contrast images of FAF. However, at the beginning of the examination, it was difficult for the examinees to gaze at the same point, and the intensity of FAF was not always sufficient to be measured. Furthermore, a 40-second exposure to the HRA2 may not be sufficient for full bleaching, especially for the cone photopigments. For these reasons, we calculated the fODD, using extrapolation by fitting a simple exponential curve. This technique was used in previous reports to estimate the optical density change during bleaching.[22,23] We were able to obtain the log[$F(\infty)$], fODD, and k values from the formula. By extrapolation, we could estimate the log[$F(\infty)$] when the log(F) reached a constant level. However, a constant level of log(F) does not denote a fully bleached condition, because the photopigment can reach equilibrium through steady state illumination. The equilibrium depends on the intensity of illumination and the chromophores.[22] The intensity of the bleaching light was different at each site that was measured, because the 488-nm bleaching light was attenuated by macular pigments. When we hypothesized that the intensity of autofluorescence was constant in all areas of the fundus, the log density difference was estimated to be approximately 0.18 to 0.30, which was the difference of log[F(end)] between the fovea and the temporal fifth grid. Although this difference is mainly thought to affect the intensity of excitation light, the contribution to autofluorescence intensity cannot be estimated because the actual distribution of fluorophore density and the coefficient for autofluorescence emission are unknown. To eliminate this problem, we could use a longer wave length for excitation. For these reasons, it is difficult to determine the abnormality of the photopigment from the actual value of fODD; the map of fODD was thus created to detect the abnormality of the photopigment. When interpreting the map of fODD, one should take into consideration the influence of the macular pigment. Previous reports assessing optical density differences used the difference of the logarithmic value of the pixel.[13,24] As it is difficult to align the pictures on a pixel-to-pixel basis using this method, we measured multiple regions of interest and reconstructed a false-color map for the evaluation of the fODD.

Normal Data

The mean ± SD of 90 pixels temporal to the fovea were 0.096 ± 0.035. The fODD value was approximately 50% of that reported in previous studies using autofluorescence densitometry or reflectometry.[12,17] This difference may depend on the eccentricity of the measurement or the wavelength. The distribution patterns of FAF in the bleached condition on the vertical and horizontal lines were similar to those reported by Delori et al.[25] The fODD also showed a concentric pattern, and the fODD value in the superior retina was higher than that in the inferior retina. Because the mapping data for the fODD in 9 × 9 grids exhibited remarkable similarity to the patterns of the rod photoreceptor, it appeared mainly to represent the distribution of the optical density difference of the rods. The fODD was higher in the superior retina than in the inferior retina in the present study. A reduction of the anatomic rod density in the inferior retina with age is consistent with our results.[26] Because the excitation laser at 488 nm contributed to the results of the fODD, the absorption of the macular pigment must be considered when interpreting these data. The fODD at the center of the grids did not reach 0 in 12 sessions in six eyes. The lipofuscin excited by 488-nm light generates autofluorescence between 500 and 750 nm.[27–29] As the barrier filter of the HRA2 passes light of >500 nm, the fODD should be affected not only by rod pigments but also by cone pigments. The fODD of cones and rods is influenced mainly by the excitation light

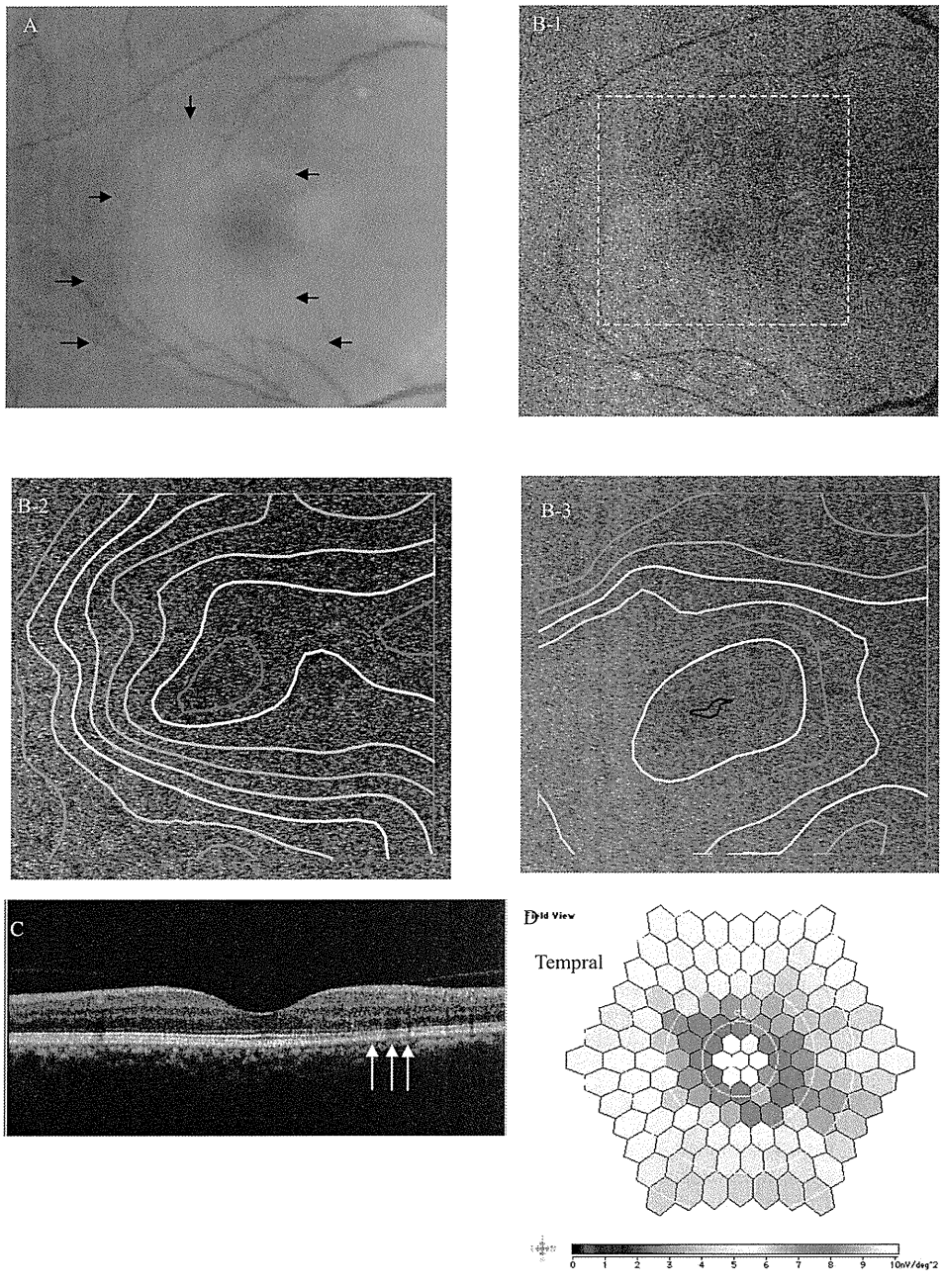

FIGURE 7. A 58-year-old man 10 months after the onset of CSC. (**A**) Color fundus photograph at the first visit showing SRD (*arrows*). (**B-1**) FAF image after resolution of SRD at the examination. *Dashed line*: the area of the measurement. (**B-2**) Overlay image of map of maximum intensity of autofluorescence (log[*F*(end)]). The intensity of autofluorescence increased from the center of the fovea to the lower temporal area. (**B-3**) Overlay image of map of fODD. The fODD decreased in the area showing hyperautofluorescence. (**C**) Vertical slice of SD-OCT image through the fovea. The intensity of the signal of the IS/OS line was attenuated in the area of hyperautofluorescence (*white arrows*). (**D**) Multifocal electroretinogram recorded at the same visit. The amplitude decreased from the temporal to inferior retina, where the response of fODD decreased.

(488 nm) rather than the emitted autofluorescence, the latter of which is not guided by the photoreceptors for cones and is absorbed less by rods.[17]

Eyes with Diseases

When the fODD is measured, the FAF intensity from the RPE should not be changed by exposure to light, even in the damaged RPE. As the RPE cells contain a substance derived from retinol,[30] the autofluorescence intensity may change during strong exposure to light. The laser power (0.2 mW) at 488 nm for the HRA2 system was higher than that reported for conventional imaging densitometry (0.07 mW).[13] We measured the autofluorescence intensity in macular holes where the RPE was directly exposed to the light, and found that the

TABLE 3. Summary of Autofluorescence Change and fODD in Various Eye Diseases

Lesions	Response of fODD	Findings of SD-OCT	
		Inner Retina	Outer Retina
Macular hole	Absent	Absent	Absent
Photocoagulation burns	Decreased	Damaged	Damaged or absent
BRAO	Normal	Damaged	Normal
CSC	Decreased	Almost normal	Damaged

intensity of FAF decreased slightly during exposure to light (the average of the slope was −0.00039), which may have been caused by photobleaching of the fluorophores. When the RPE is covered with the sensory retina, the contribution of this effect to the results may decrease. However, the fODD could be underestimated, because of the attenuation of autofluorescence of the RPE during exposure to light.

Moderately coagulated laser burns have autofluorescence.[31] The RPE shows both proliferation and hypertrophy histopathologically.[32] To examine the autofluorescence of the damaged RPE, we measured the autofluorescence intensity in the areas of the laser burns. At the center of the moderately coagulated laser burns in the eyes with long-standing BRVO, SD-OCT revealed disruption of the IS/OS line and atrophy of the inner retina. Because the fODD was small or absent in the laser burns, the autofluorescence from the pathologic RPE did not change during the measurement. The fODD could thus be assessed for a damaged RPE. This result suggests that the integrity of the IS/OS line in SD-OCT shows a good correspondence to the fODD response.

Focal or multifocal ERG shows a reduced response in the area affected by BRAO.[33] However, SD-OCT shows a well-preserved IS/OS line in the region of artery occlusion.[34] The impact on the outer segment of the retina of BRAO remains controversial. To our knowledge, the response of the outer segment to light stimuli in eyes with BRAO has not been established. The fODD map of eyes with BRAO showed a concentric pattern similar to that in the eyes of the normal subjects. This result indicated that the function of the photopigment was preserved in eyes with long-standing BRAO, although the electrophysiological function of the photoreceptor cells was impaired. The dysfunction of the Müller cells may affect the difference between the fODD and the electrophysiological response.

CSC is thought to be an acute disorder of the choroid that causes SRD and damage to the retina. The amplitude of the electrophysiological response is attenuated in areas of resolved SRD.[35,36] The sensitivity according to the microperimeter is lower within the previously affected area of SRD.[37] Disturbance of the IS/OS line in the affected area was also demonstrated recently by SD-OCT.[38] A low fODD amplitude is consistent with these results and a previous report of conventional densitometry.[39] In the present study, the fODD decreased in the area showing hyperautofluorescence and IS/OS attenuation in the eye with CSC. The area showed a decrease of the fODD amplitude that corresponded to the area of decreased amplitude in the multifocal electroretinogram (Fig. 7D). A decrease of photopigment is considered to be one reason for electrophysiological impairment in resolved CSC.[40] The fODD is an acceptable measure with which to evaluate the photopigment abnormalities caused by disorders of the outer retina.

The photopigment could be assessed using the fODD in diseases involving the inner and outer retina (Table 3). SD-OCT can delineate anatomic disorders of the retina, including those in the outer segment of photoreceptor cells.[41–44] However, the function of the outer segment cannot be assessed by OCT. As we were able to assess focal abnormalities of the outer segment by autofluorescence, it could be useful in elucidating the mechanism of retinal diseases in combination with SD-OCT.

The main weaknesses of densitometry by autofluorescence are the difficulty of quantifying the amplitude of the optical density differences of photopigments due to interindividual variations in the autofluorescence and the limitations of the measurements in cases of weak FAF. These problems may be improved by using a longer wavelength laser for emission. The fODD should be affected by the optical density differences of both cone pigments and rod pigments, because of the filter set of the HRA2 system. We could not distinguish whether changes of the cone pigments or the rod pigments contributed to the fODD. Moreover, absorption by the macular pigments may have affected the fODD. However, we believe that the fODD is useful for evaluating the photopigments clinically, because it can indicate abnormalities through a comparison of the distributions on the map. In particular, the fODD is useful for investigating the relationship between autofluorescence abnormalities and photopigments.

In conclusion, we showed that densitometry with a commercially available SLO system was suitable for assessing focal abnormalities of photopigments in eyes with retinal diseases. This method may also be useful for the assessment of macular diseases clinically.

References

1. Vaclavik V, Vujosevic S, Dandekar SS, Bunce C, Peto T, Bird AC. Autofluorescence imaging in age-related macular degeneration complicated by choroidal neovascularization: a prospective study. *Ophthalmology.* 2008;115:342–346.
2. Smith RT, Chan JK, Busuoic M, Sivagnanavel V, Bird AC, Chong NV. Autofluorescence characteristics of early, atrophic, and high-risk fellow eyes in age-related macular degeneration. *Invest Ophthalmol Vis Sci.* 2006;47:5495–5504.
3. Schmitz-Valckenberg S, Bultmann S, Dreyhaupt J, Bindewald A, Holz FG, Rohrschneider K. Fundus autofluorescence and fundus perimetry in the junctional zone of geographic atrophy in patients with age-related macular degeneration. *Invest Ophthalmol Vis Sci.* 2004;45:4470–4476.
4. Holz FG, Bindewald-Wittich A, Fleckenstein M, Dreyhaupt J, Scholl HP, Schmitz-Valckenberg S. Progression of geographic atrophy and impact of fundus autofluorescence patterns in age-related macular degeneration. *Am J Ophthalmol.* 2007;143:463–472.
5. Delori FC, Dorey CK, Staurenghi G, Arend O, Goger DG, Weiter JJ. In vivo fluorescence of the ocular fundus exhibits retinal pigment epithelium lipofuscin characteristics. *Invest Ophthalmol Vis Sci.* 1995;36:718–729.
6. Eldred GE, Katz ML. Fluorophores of the human retinal pigment epithelium: separation and spectral characterization. *Exp Eye Res.* 1988;47:71–86.
7. Framme C, Roider J. Fundus autofluorescence in macular hole surgery. *Ophthalmic Surg Lasers.* 2001;32:383–390.
8. Sayanagi K, Ikuno Y, Tano Y. Different fundus autofluorescence patterns of retinoschisis and macular hole retinal detachment in high myopia. *Am J Ophthalmol.* 2007;144:299–301.
9. Alpern M, Pugh EN Jr. The density and photosensitivity of human rhodopsin in the living retina. *J Physiol.* 1974;237:341–370.
10. Rushton WA, Campbell FW. Measurement of rhodopsin in the living human eye. *Nature.* 1954;174:1096–1097.
11. van Norren D, van der Kraats J. A continuously recording retinal densitometer. *Vision Res.* 1981;21:897–905.
12. Liem AT, Keunen JE, van Norren D, van de Kraats J. Rod densitometry in the aging human eye. *Invest Ophthalmol Vis Sci.* 1991;32:2676–2682.
13. Tornow RP, Stilling R, Zrenner E. Scanning laser densitometry and color perimetry demonstrate reduced photopigment density and sensitivity in two patients with retinal degeneration. *Vision Res.* 1999;39:3630–3641.
14. Kemp CM, Faulkner DJ. Rhodopsin measurement in human disease: fundus reflectometry using television. *Dev Ophthalmol.* 1981;2:130–134.
15. Elsner AE, Burns SA, Beausencourt E, Weiter JJ. Foveal cone photopigment distribution: small alterations associated with macular pigment distribution. *Invest Ophthalmol Vis Sci.* 1998;39:2394–2404.
16. Hood C, Rushton WA. The Florida retinal densitometer. *J Physiol.* 1971;217:213–229.
17. Prieto PM, McLellan JS, Burns SA. Investigating the light absorption in a single pass through the photoreceptor layer by means of the lipofuscin fluorescence. *Vision Res.* 2005;45:1957–1965.

18. van Norren D, van de Kraats J. Imaging retinal densitometry with a confocal scanning laser ophthalmoscope. *Vision Res.* 1989;29: 1825–1830.
19. Spaide RF. Fundus autofluorescence and age-related macular degeneration. *Ophthalmology.* 2003;110:392–399.
20. Scholl HP, Chong NH, Robson AG, Holder GE, Moore AT, Bird AC. Fundus autofluorescence in patients with Leber congenital amaurosis. *Invest Ophthalmol Vis Sci.* 2004;45:2747–2752.
21. Theelen T, Berendschot TT, Boon CJ, Hoyng CB, Klevering BJ. Analysis of visual pigment by fundus autofluorescence. *Exp Eye Res.* 2008;86:296–304.
22. Alpern M. Rhodopsin kinetics in the human eye. *J Physiol.* 1971; 217:447–471.
23. Rushton WA, Baker HD. Effect of a very bright flash on cone vision and cone pigments in man. *Nature.* 1963;200:421–423.
24. Wustemeyer H, Moessner A, Jahn C, Wolf S. Macular pigment density in healthy subjects quantified with a modified confocal scanning laser ophthalmoscope. *Graefes Arch Clin Exp Ophthalmol.* 2003;241:647–651.
25. Delori FC, Goger DG, Dorey CK. Age-related accumulation and spatial distribution of lipofuscin in RPE of normal subjects. *Invest Ophthalmol Vis Sci.* 2001;42:1855–1866.
26. Curcio CA, Sloan KR, Kalina RE, Hendrickson AE. Human photoreceptor topography. *J Comp Neurol.* 1990;292:497–523.
27. Wihlmark U, Wrigstad A, Roberg K, Brunk UT, Nilsson SE. Lipofuscin formation in cultured retinal pigment epithelial cells exposed to photoreceptor outer segment material under different oxygen concentrations. *APMIS.* 1996;104:265–271.
28. Haralampus-Grynaviski NM, Lamb LE, Clancy CM, et al. Spectroscopic and morphological studies of human retinal lipofuscin granules. *Proc Natl Acad Sci USA.* 2003;100:3179–3184.
29. Rozanowska M, Pawlak A, Rozanowski B, et al. Age-related changes in the photoreactivity of retinal lipofuscin granules: role of chloroform-insoluble components. *Invest Ophthalmol Vis Sci.* 2004;45:1052–1060.
30. Katz ML, Gao CL. Vitamin A incorporation into lipofuscin-like inclusions in the retinal pigment epithelium. *Mech Ageing Dev.* 1995;84:29–38.
31. Framme C, Brinkmann R, Birngruber R, Roider J. Autofluorescence imaging after selective RPE laser treatment in macular diseases and clinical outcome: a pilot study. *Br J Ophthalmol.* 2002;86:1099–1106.
32. Stitt AW, Gardiner TA, Archer DB. Retinal and choroidal responses to panretinal photocoagulation: an ultrastructural perspective. *Graefes Arch Clin Exp Ophthalmol.* 1995;233:699–705.
33. Kondo M, Miyake Y, Horiguchi M, Suzuki S, Tanikawa A. Clinical evaluation of multifocal electroretinogram. *Invest Ophthalmol Vis Sci.* 1995;36:2146–2150.
34. Karacorlu M, Ozdemir H, Arf Karacorlu S. Optical coherence tomography findings in branch retinal artery occlusion. *Eur J Ophthalmol.* 2006;16:352–353.
35. Moschos M, Brouzas D, Koutsandrea C, Stefanos B, Loukianou H, Papantonis F. Assessment of central serous chorioretinopathy by optical coherence tomography and multifocal electroretinography. *Ophthalmologica.* 2007;221:292–298.
36. Suzuki K, Hasegawa S, Usui T, et al. Multifocal electroretinogram in patients with central serous chorioretinopathy. *Jpn J Ophthalmol.* 2002;46:308–314.
37. Ojima Y, Tsujikawa A, Hangai M, et al. Retinal sensitivity measured with the micro perimeter 1 after resolution of central serous chorioretinopathy. *Am J Ophthalmol.* 2008;146:77–84.
38. Ojima Y, Hangai M, Sasahara M, et al. Three-dimensional imaging of the foveal photoreceptor layer in central serous chorioretinopathy using high-speed optical coherence tomography. *Ophthalmology.* 2007;114:2197–2207.
39. Chuang EL, Sharp DM, Fitzke FW, Kemp CM, Holden AL, Bird AC. Retinal dysfunction in central serous retinopathy. *Eye.* 1987;1(1): 120–125.
40. Chappelow AV, Marmor MF. Multifocal electroretinogram abnormalities persist following resolution of central serous chorioretinopathy. *Arch Ophthalmol.* 2000;118:1211–1215.
41. Koizumi H, Spaide RF, Fisher YL, Freund KB, Klancnik JM Jr, Yannuzzi LA. Three-dimensional evaluation of vitreomacular traction and epiretinal membrane using spectral-domain optical coherence tomography. *Am J Ophthalmol.* 2008;145:509–517.
42. Sakamoto A, Hangai M, Yoshimura N. Spectral-domain optical coherence tomography with multiple B-scan averaging for enhanced imaging of retinal diseases. *Ophthalmology.* 2008;115: 1071–1078.e7.
43. Srinivasan VJ, Ko TH, Wojtkowski M, et al. Noninvasive volumetric imaging and morphometry of the rodent retina with high-speed, ultrahigh-resolution optical coherence tomography. *Invest Ophthalmol Vis Sci.* 2006;47:5522–5528.
44. Wojtkowski M, Srinivasan V, Fujimoto JG, et al. Three-dimensional retinal imaging with high-speed ultrahigh-resolution optical coherence tomography. *Ophthalmology.* 2005;112:1734–1746.

Comparison of Intravitreal Triamcinolone Acetonide With Photodynamic Therapy and Intravitreal Bevacizumab with Photodynamic Therapy for Retinal Angiomatous Proliferation

MASAAKI SAITO, CHIEKO SHIRAGAMI, FUMIO SHIRAGA, MARIKO KANO, AND TOMOHIRO IIDA

• PURPOSE: To compare the efficacy of combined therapy with intravitreal triamcinolone (IVTA) and photodynamic therapy (PDT; IVTA plus PDT) with intravitreal bevacizumab (IVB) and PDT (IVB plus PDT) for patients with retinal angiomatous proliferation (RAP).

• DESIGN: Retrospective, observational case series.

• METHODS: We retrospectively reviewed 25 treatment-naïve eyes of 22 Japanese patients (11 men, 11 women) with retinal angiomatous proliferation. Twelve eyes of 11 patients were treated with combined therapy of IVTA plus PDT from September 1, 2004, through July 31, 2006. Thirteen eyes of 11 patients were treated with combined therapy of IVB plus PDT from February 1, 2007, through January 31, 2008.

• RESULTS: In 12 eyes treated with IVTA plus PDT, the mean best-corrected visual acuity (BCVA) levels at baseline and 12 months were 0.29 and 0.13, respectively. A significant ($P < .05$) decline in the mean BCVA from baseline was observed at 12 months. In 13 eyes treated with IVB plus PDT, the mean BCVA levels at baseline and 12 months were 0.25 and 0.37. A significant ($P < .05$) improvement in the mean BCVA from baseline was observed. At 12 months, the difference in BCVA between the 2 groups was significant ($P < .05$). The mean numbers of treatments at 12 months in the IVTA plus PDT group and the IVB plus PDT group were 2.7 and 1.6, respectively. The difference between the 2 treatments reached significance ($P < .05$). No complications developed.

• CONCLUSIONS: Compared with IVTA plus PDT, IVB plus PDT was significantly more effective in maintaining and improving visual acuity and in reducing the number of treatment for patients with retinal angiomatous proliferation. (Am J Ophthalmol 2010;149: 472–481. © 2010 by Elsevier Inc. All rights reserved.)

Accepted for publication Sep 21, 2009.

From the Department of Ophthalmology, Fukushima Medical University School of Medicine, Fukushima, Japan (M.S., M.K., T.I.); and the Department of Ophthalmology, Kagawa University, Kagawa, Japan (C.S., F.S.).

Inquiries to Masaaki Saito, Department of Ophthalmology, Fukushima Medical University School of Medicine, 1 Hikarigaoka, Fukushima 960-1295, Japan; e-mail: smasaaki@fmu.ac.jp

RETINAL ANGIOMATOUS PROLIFERATION (RAP) HAS been described as a variant of exudative age-related macular degeneration (AMD).[1] The term RAP was first coined by Yannuzzi and associates in 2001.[1] RAP is differentiated into 3 stages based on clinical and angiographic observations: stage 1, proliferation of intraretinal capillaries originating from the deep retinal complex (intraretinal neovascularization); stage 2, growth of the retinal vessels into the subretinal space (subretinal neovascularization); and stage 3, clinically or angiographically observed choroidal neovascularization (CNV).[1] RAP sometimes is referred to as type 3 neovascularization to distinguish it from the type 1 and 2 CNV anatomic classifications described by Freund and associates.[2]

RAP represents 15% of all neovascular AMD in white patients and 4.5% of all neovascular AMD in Japanese patients.[3,4] The natural course of RAP differs from typical exudative AMD and has poor visual outcomes.[5–7] Furthermore, various treatments for RAP such as conventional laser photocoagulation,[6,8] transpupillary thermotherapy,[6,9] surgical ablation,[10,11] and monotherapy of photodynamic therapy (PDT) with verteporfin (Visudyne; Novartis Pharma AG, Basel, Switzerland)[12,13] have not been efficacious.

CNV complexes are comprised of inflammatory cells and vascular endothelial growth factor (VEGF).[14–16] Corticosteroids such as triamcinolone acetonide (TA) have antiangiogenic, antiinflammatory, and anti-VEGF effects.[17,18] Recent studies have reported that combined therapy of intravitreal TA (IVTA) and PDT for RAP effectively resolves angiographic leakage and maintains or improves visual acuity (VA).[19,20]

Anti-VEGF therapy prevents formation of CNV and decreases leakage from existing CNV in animal models.[21] VEGF monoclonal antibodies and aptamers such as ranibizumab (Lucentis; Genentech, Inc, South San Francisco, California, USA), bevacizumab (Avastin; Genentech), and pegaptanib (Macugen; EyeTech Pharmaceuticals, Lexington, Massachusetts, USA) reduce vascular leakage and improve visual outcomes in patients with CNV secondary to AMD.[22–25] Moreover, combined therapy of intravitreal bevacizumab (IVB) injections and PDT administered to treat CNV reduced the retreatment rates in patients with AMD.[26–28] We reported recently that combined therapy of IVB and PDT was effective for treating RAP after 6

0002-9394/10/$36.00
doi:10.1016/j.ajo.2009.09.016

TABLE 1. Intravitreal Triamcinolone Acetonide and Photodynamic Therapy for Retinal Angiomatous Proliferation

						Baseline					12 Months after Treatment					
Case No.	Age (yrs)	Gender	Eye	RAP Stage	Lens Status	VA	Central Retinal Thickness (μm)	RRA	GLD (μm)	IOP (mmHg)	VA	Central Retinal Thickness (μm)	RRA	GLD (μm)	IOP (mmHg)	No. Treatments
1	74	F	Right	2+PED	Phakic eye	0.8	279	Yes	1590	13	0.8	34	No	0	12	1
2	85	F	Right	2	Pseudophakia	0.2	385	Yes	1100	13	0.1	115	Yes	0	11	2
3	86	M	Right	2	Phakic eye	0.4	293	Yes	2570	10	0.1	550	Yes	2197	10	4
4	86	M	Left	2+PED	Phakic eye	0.3	350	Yes	1080	11	0.2	289	Yes	957	11	4
5	74	F	Left	2	Pseudophakia	0.8	542	Yes	3600	13	0.5	232	No	0	12	3
6	63	M	Right	2+PED	Phakic eye	0.8	267	Yes	5610	17	0.06	481	Yes	4784	18	3
7	84	F	Right	2+PED	Phakic eye	0.6	355	Yes	2690	10	0.08	407	Yes	3296	9	5
8	90	F	Right	2	Pseudophakia	0.3	314	No	4516	13	0.03	83	—	0	16	1
9	70	F	Left	2	Pseudophakia	0.09	367	Yes	2450	16	0.2	324	Yes	0	19	2
10	69	F	Right	2	Phakic eye	0.15	625	Yes	3334	14	0.1	135	Yes	0	10	3
11	68	M	Right	2	Pseudophakia	0.1	521	Yes	3430	20	0.3	237	Yes	0	16	2
12	90	F	Right	2+PED	Pseudophakia	0.1	575	Yes	2648	14	0.05	423	Yes	0	15	2
Mean	78	—	—	—	—	0.29	406	—	2885	13.7	0.13	276	—	936	13.3	2.7
SD	9.5	—	—	—	—	—	125	—	1335	2.9	—	166	—	1623	3.4	1.2

F = female; GLD = greatest linear dimension; IOP = intraocular pressure; M = male; PED = pigment epithelial detachment; RAP = retinal angiomatous proliferation; RRA = retinal–retinal anastomosis; SD = standard deviation; VA = decimal visual acuity; yrs = years.

TABLE 2. Intravitreal Bevacizumab and Photodynamic Therapy for Retinal Angiomatous Proliferation

						Baseline					12 Months after Treatment					
Case No.	Age (yrs)	Gender	Eye	RAP Stage	Lens Status	VA	Central Retinal Thickness (μm)	RRA	GLD (μm)	IOP (mmHg)	VA	Central Retinal Thickness (μm)	RRA	GLD (μm)	IOP (mmHg)	No. Treatments
13	64	F	Right	2	Phakic eye	1.0	234	No	602	16	1.0	117	—	0	12	2
14	63	M	Right	2+PED	Phakic eye	0.07	601	Yes	4331	12	0.2	126	No	0	10	2
15	81	M	Right	2	Phakic eye	0.4	393	No	1900	15	1.0	124	—	0	13	1
16	78	M	Left	2	Phakic eye	0.6	406	No	1998	11	1.2	125	—	0	11	1
17	89	M	Left	2+PED	Pseudophakia	0.3	379	Yes	3531	16	0.6	182	No	0	13	1
18	87	F	Right	3	Pseudophakia	0.06	394	Yes	2368	10	0.07	140	Yes	0	10	1
19	87	F	Left	2+PED	Pseudophakia	0.7	396	Yes	5532	10	0.7	112	Yes	0	10	2
20	78	M	Left	2	Phakic eye	0.9	430	Yes	975	15	0.8	127	No	0	14	2
21	83	F	Right	2	Phakic eye	0.05	514	Yes	3489	19	0.05	88	No	0	14	2
22	83	F	Left	2+PED	Pseudophakia	0.3	479	Yes	4568	17	0.6	44	No	0	16	3
23	72	M	Right	2+PED	Phakic eye	0.3	360	Yes	3300	16	0.2	74	No	0	13	2
24	74	M	Right	3	Phakic eye	0.06	950	Yes	4494	15	0.09	426	No	0	11	1
25	79	M	Left	2+PED	Pseudophakia	0.3	389	Yes	3321	11	0.9	66	No	0	10	1
Mean	78	—	—	—	—	0.25	456	—	3108	14.1	0.37	135	—	0	12.1	1.6
SD	8.2	—	—	—	—	—	171	—	1469	2.9	—	94	—	—	1.9	0.7

F = female; GLD = greatest linear dimension; M = male; PED = pigment epithelial detachment; RAP = retinal angiomatous proliferation; RRA = retinal–retinal anastomosis; SD = standard deviation; VA = decimal visual acuity; yrs = years.

months of follow-up.[29] The purpose of the current study was to clarify the efficiency of combined therapy of IVB plus PDT compared with combined therapy of IVTA plus PDT for treating patients with RAP over 12 months.

METHODS

WE RETROSPECTIVELY REVIEWED 25 EYES OF 22 JAPANESE patients (11 men, 11 women; age range, 63 to 90 years; mean ± standard deviation, 78.3 ± 8.8 years) with RAP. Twelve eyes of 11 patients (3 men, 8 women; age range, 63 to 90 years; mean age, 78.3 years) were treated with combined therapy of IVTA plus PDT from September 1, 2004, through July 31, 2006. Thirteen eyes of 11 patients (8 men, 3 women; age range, 63 to 89 years; mean age, 78.3 years) were treated with combined therapy of IVB and PDT from February 1, 2007, through January 31, 2008. The 6-month results for 8 of the 13 eyes treated with IVB plus PDT were reported previously.[29] The patients were followed up for at least 12

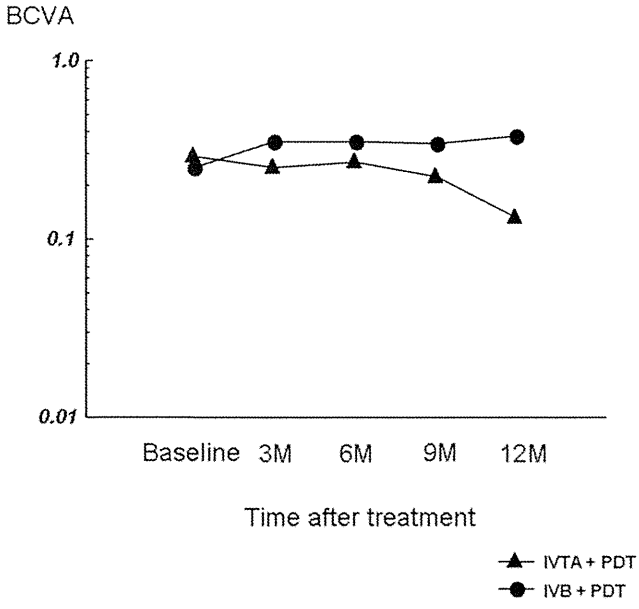

FIGURE 1. Graph showing results of intravitreal triamcinolone acetonide with photodynamic therapy (IVTA plus PDT) and intravitreal bevacizumab with photodynamic therapy (IVB plus PDT) for retinal angiomatous proliferation (RAP). In eyes treated with IVTA plus PDT, there is a significant ($P < .05$, paired t test) decline in the mean best-corrected visual acuity (BCVA) between baseline and 12 months. In eyes treated with IVB plus PDT, there is a significant improvement in the mean BCVA between baseline and 3, 6, and 12 months ($P < .01$, $P < .05$, $P < .05$, respectively, paired t test). There is no significant ($P = .74$) difference in the mean BCVA between groups at baseline; nevertheless, there is a significant difference in the mean BCVA at 12 months ($P < .05$, nonpaired t test) between the IVB plus PDT group and the IVTA plus PDT group. M = month(s).

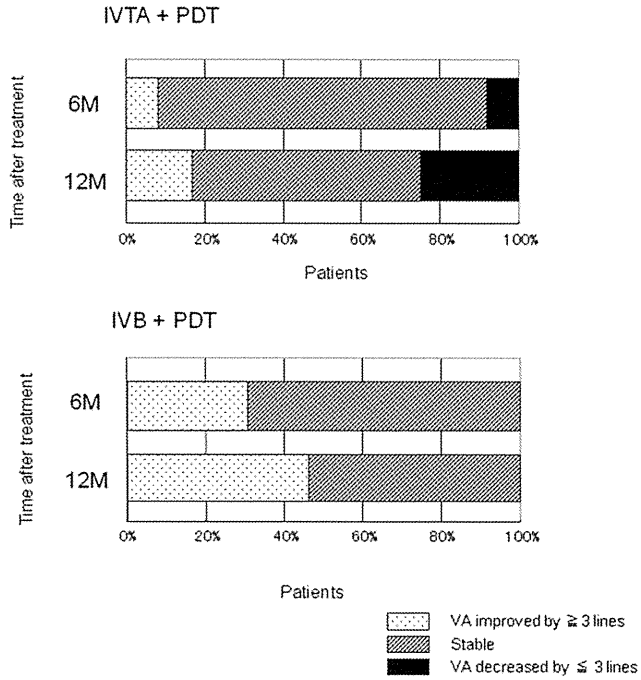

FIGURE 2. The distribution of the mean best-corrected visual acuity (BCVA) changes from baseline after treatment with combined intravitreal triamcinolone acetonide with photodynamic therapy (IVTA plus PDT) and intravitreal bevacizumab with photodynamic therapy (IVB plus PDT). (Top) One and 3 eyes treated with IVTA plus PDT had decreased BCVA at 6 and 12 months, respectively. (Bottom) No eyes treated with IVB plus PDT had decreased BCVA of 3 lines or more after treatment over 12 months. M = month(s).

months at Fukushima Medical University Hospital or Kagawa University Hospital. No patient had undergone a previous treatment. The treatment was approved by the Institutional Review Boards/Ethics Committees at Fukushima Medical University and Kagawa University. After the potential risks and benefits were explained in detail, all patients provided written informed consent. The exclusion criteria were previous treatment for RAP such as laser photocoagulation, submacular surgery, transpupillary thermotherapy, and PDT; glaucoma; tears in the retinal pigment epithelium; and maculopathies such as diabetic maculopathy, retinal vascular occlusion, or idiopathic juxtafoveal retinal telangiectasis.

We recorded the best-corrected visual acuity (BCVA) measured with a Japanese standard decimal VA chart and calculated the mean BCVA using the logarithm of the minimal angle of resolution (logMAR) scale. All patients underwent a standardized examination including slit-lamp biomicroscopy with a contact lens, fundus color photography, fluorescein angiography (FA), and indocyanine green angiography (ICGA) with a fundus camera (TRC-50 FA/IA/IMAGEnet H1024 system; Topcon, Tokyo, Japan), with a confocal scanning laser ophthalmoscope (Heidelberg Retina Angiograph 2; Heidelberg Engineering, Heidelberg, Germany), or both. All examinations were performed using time-domain optical coherence tomography (OCT; OCT 3000; Carl Zeiss, Meditec, Dublin, California, USA; or OCT-Ophthalmoscope; Nidek-OTI, Gamagori, Japan) in eyes treated with IVTA plus PDT and spectral-domain OCT (3D-OCT; Topcon; or Cirrus OCT, Carl Zeiss) in eyes treated with IVB plus PDT. All patients were examined using the same OCT machine during the follow-up. FA was performed to determine the lesion type, the location, and the activity of the RAP lesions. ICGA was performed to diagnose RAP and to identify retinal–retinal anastomosis. The central retinal thickness, defined as the distance from the retinal pigment epithelium to the inner limiting membrane, was measured at baseline and at 3, 6, 9, and 12 months after treatment using internal caliper software.

All patients had documented visual loss before treatment. IVTA (4 mg/0.1 mL) or IVB (1.25 mg/0.05 mL) was injected 3.5 to 4.0 mm posterior to the corneal limbus into the vitreous cavity using a 27-gauge needle after topical anesthesia was applied. In the patients treated with IVTA plus PDT, PDT was performed 7 days after IVTA was injected. In the patients treated with IVB plus PDT, PDT was administered 1